5 Seismic refraction surveying

5.1 Introduction

The seismic refraction surveying method uses seismic energy that returns to the surface after travelling through the ground along refracted ray paths. As briefly discussed in Chapter 3, the first arrival of seismic energy at a detector offset from a seismic source always represents either a direct ray or a refracted ray. This fact allows simple refraction surveys to be performed in which attention is concentrated solely on the first arrival (or *onset*) of seismic energy, and time–distance plots of these first arrivals are interpreted to derive information on the depth to refracting interfaces. As is seen later in the chapter, this simple approach does not always yield a full or accurate picture of the subsurface. In such circumstances more complex interpretations may be applied. The method is normally used to locate refracting interfaces (refractors) separating layers of different seismic velocity, but the method is also applicable in cases where velocity varies smoothly as a function of depth or laterally.

Refraction seismograms may also contain reflection events as subsequent arrivals, though generally no special attempt is made to enhance reflected arrivals in refraction surveys. Nevertheless, the relatively high reflection coefficients associated with rays incident on an interface at angles near to the critical angle often lead to strong *wide-angle reflections* which are quite commonly detected at the greater recording ranges that characterize large-scale refraction surveys. These wide-angle reflections often provide valuable additional information on subsurface structure such as, for example, indicating the presence of a low-velocity layer which would not be revealed by refracted arrivals alone.

The vast majority of refraction surveying is carried out along profile lines which are arranged to be sufficiently long to ensure that refracted arrivals from target layers are recorded as first arrivals for at least half the length of the line. Refraction profiles typically need to be between five and ten times as long as the required depth of investigation. A consequence of this requirement is that large seismic sources are needed for the detection of deep refractors in order that sufficient energy is transmitted over the long range necessary for the recording of deep refracted phases as first arrivals. The profile length required in any particular survey depends upon the distribution of velocities with depth at that location. The requirement in refraction surveying for an increase in profile length with increase in the depth of investigation contrasts with the situation in conventional reflection surveying, where near-normal incidence reflections from deep interfaces are recorded at small offset distances.

Refraction seismology is applied to a very wide range of scientific and technical problems, from engineering site investigation surveys to large-scale experiments designed to study the structure of the entire crust or lithosphere. Refraction measurements can provide valuable velocity information for use in the interpretation of reflection surveys, and refracted arrivals recorded during land reflection surveys are used to map the weathered layer, as discussed in Chapter 4. This wide variety of applications leads to an equally wide variety of field survey methods and associated interpretation techniques.

In many geological situations, subsurface refractors may approximate planar surfaces over the linear extent of a refraction line. In such cases the observed travel-time plots are commonly assumed to be derived from a set of planar layers and are analysed to determine depths to, and dips of, individual planar refractors. The geometry of refracted ray paths through planar layer models of the subsurface is considered first, after which consideration is given to methods of dealing with refraction at irregular (non-planar) interfaces.

5.2 Geometry of refracted ray paths: planar interfaces

The general assumptions relating to the ray path

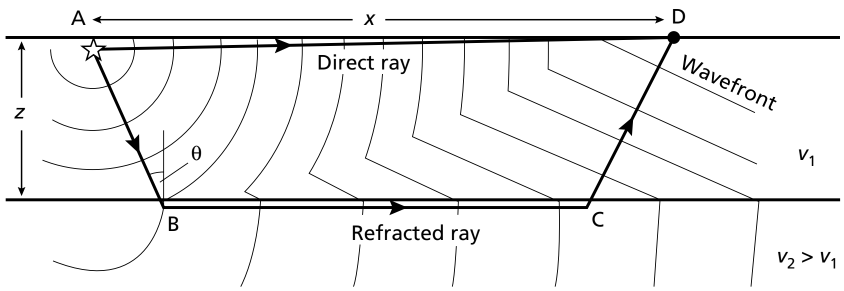

Fig. 5.1 Successive positions of the expanding wavefronts for direct and refracted waves through a two-layer model. Only the wavefront of the first arrival phase is shown. Individual ray paths from source A to detector D are drawn as solid lines.

geometries considered below are that the subsurface is composed of a series of layers, separated by planar and possibly dipping interfaces. Also, within each layer seismic velocities are constant, and the velocities increase with layer depth. Finally, the ray paths are restricted to a vertical plane containing the profile line (i.e. there is no component of cross-dip).

5.2.1 Two-layer case with horizontal interface

Figure 5.1 illustrates progressive positions of the wavefront from a seismic source at A associated with energy travelling directly through an upper layer and energy critically refracted in a lower layer. Direct and refracted ray paths to a detector at D, a distance x from the source, are also shown. The layer velocities are v_1 and v_2 ($>v_1$) and the refracting interface is at a depth z.

The direct ray travels horizontally through the top of the upper layer from A to D at velocity v_1. The refracted ray travels down to the interface and back up to the surface at velocity v_1 along slant paths AB and CD that are inclined at the critical angle θ, and travels along the interface between B and C at the higher velocity v_2. The total travel time along the refracted ray path ABCD is

$$\begin{aligned} t &= t_{AB} + t_{BC} + t_{CD} \\ &= \frac{z}{v_1 \cos\theta} + \frac{(x - 2z\tan\theta)}{v_2} + \frac{z}{v_1\cos\theta} \end{aligned}$$

Noting that $\sin\theta = v_1/v_2$ (Snell's Law) and $\cos\theta = (1 - v_1^2/v_2^2)^{1/2}$, the travel-time equation may be expressed in a number of different forms, a useful general form being

$$t = \frac{x}{v_2} + \frac{2z\cos\theta}{v_1} \tag{5.1}$$

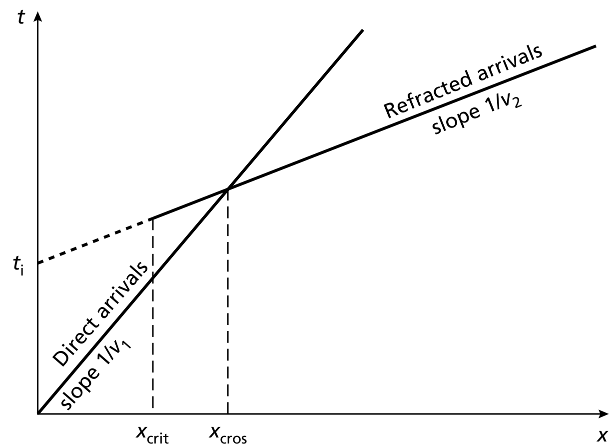

Fig. 5.2 Travel-time curves for the direct wave and the head wave from a single horizontal refractor.

Alternatively

$$t = \frac{x}{v_2} + \frac{2z\left(v_2^2 - v_1^2\right)^{1/2}}{v_1 v_2} \tag{5.2}$$

or

$$t = \frac{x}{v_2} + t_i \tag{5.3}$$

where, plotting t against x (Fig. 5.2), t_i is the intercept on the time axis of a travel-time plot or *time–distance plot* having a gradient of $1/v_2$. The *intercept time* t_i, is given by

$$t_i = \frac{2z\left(v_2^2 - v_1^2\right)^{1/2}}{v_1 v_2} \qquad \text{(from (5.2))}$$

Solving for refractor depth

$$z = \frac{t_i v_1 v_2}{2(v_2^2 - v_1^2)^{1/2}}$$

A useful way to consider the equations (5.1) to (5.3) is to note that the total travel time is the time that would have been taken to travel the total range x at the refractor velocity v_2 (that is x/v_2), plus an additional time to allow for the time it takes the wave to travel down to the refractor from the source, and back up to the receiver. The concept of regarding the observed time as a refractor travel-time plus *delay times* at the source and receiver is explored later.

Values of the best-fitting plane layered model parameters, v_1, v_2 and z, can be determined by analysis of the travel-time curves of direct and refracted arrivals:

- v_1 and v_2 can be derived from the reciprocal of the gradient of the relevant travel-time segment, see Fig. 5.2
- the refractor depth, z, can be determined from the intercept time t_i.

At the crossover distance x_{cros} the travel times of direct and refracted rays are equal

$$\frac{x_{cros}}{v_1} = \frac{x_{cros}}{v_2} + \frac{2z(v_2^2 - v_1^2)^{1/2}}{v_1 v_2}$$

Thus, solving for x_{cros}

$$x_{cros} = 2z\left[\frac{v_2 + v_1}{v_2 - v_1}\right]^{1/2} \qquad (5.4)$$

From this equation it may be seen that the crossover distance is always greater than twice the depth to the refractor. Also the crossover distance equation (5.4) provides an alternative method of calculating z.

5.2.2 Three-layer case with horizontal interface

The geometry of the ray path in the case of critical refraction at the second interface is shown in Fig. 5.3. The seismic velocities of the three layers are v_1, v_2 ($>v_1$) and v_3 ($>v_2$). The angle of incidence of the ray on the upper interface is θ_{13} and on the lower interface is θ_{23} (critical angle). The thicknesses of layers 1 and 2 are z_1 and z_2 respectively.

By analogy with equation (5.1) for the two-layer case, the travel time along the refracted ray path ABCDEF to an offset distance x, involving critical refraction at the second interface, can be written in the form

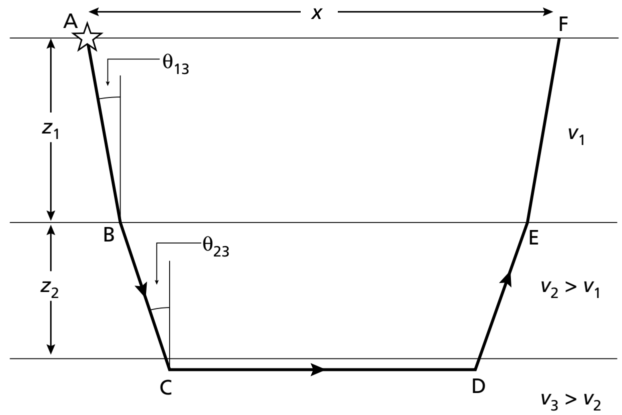

Fig. 5.3 Ray path for a wave refracted through the bottom layer of a three-layer model.

$$t = \frac{x}{v_3} + \frac{2z_1\cos\theta_{13}}{v_1} + \frac{2z_2\cos\theta_{23}}{v_2} \qquad (5.5)$$

where

$$\theta_{13} = \sin^{-1}(v_1/v_3); \quad \theta_{23} = \sin^{-1}(v_2/v_3)$$

and the notation subscripts for the angles relate directly to the velocities of the layers through which the ray travels at that angle (θ_{13} is the angle of the ray in layer 1 which is critically refracted in layer 3).

Equation (5.5) can also be written

$$t = \frac{x}{v_3} + t_1 + t_2 \qquad (5.6)$$

where t_1 and t_2 are the times taken by the ray to travel through layers 1 and 2 respectively (see Fig. 5.4).

The interpretation of travel-time curves for a three-layer case starts with the initial interpretation of the top two layers. Having used the travel-time curve for rays critically refracted at the upper interface to derive z_1 and v_2, the travel-time curve for rays critically refracted at the second interface can be used to derive z_2 and v_3 using equations (5.5) and (5.6) or equations derived from them.

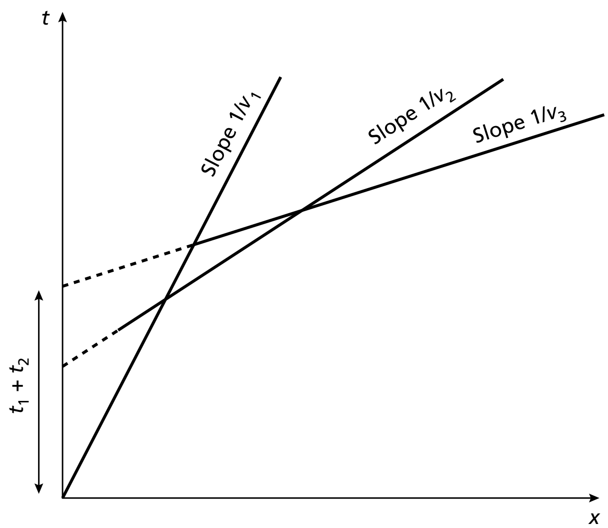

Fig. 5.4 Travel-time curves for the direct wave and the head waves from two horizontal refractors.

5.2.3 Multilayer case with horizontal interfaces

In general the travel time t_n of a ray critically refracted along the top surface of the nth layer is given by

$$t_n = \frac{x}{v_n} + \sum_{i=1}^{n-1} \frac{2z_i \cos\theta_{in}}{v_i} \tag{5.7}$$

where

$$\theta_{in} = \sin^{-1}(v_i/v_n)$$

Equation (5.7) can be used progressively to compute layer thicknesses in a sequence of horizontal strata represented by travel-time curves of refracted arrivals. In practice as the number of layers increases it becomes more difficult to identify each of the individual straight-line segments of the travel-time plot. Additionally, with increasing numbers of layers, there is less likelihood that each layer will be bounded by strictly planar horizontal interfaces, and a more complex model may be necessary. It would be unusual to make an interpretation using this method for more than four layers.

5.2.4 Dipping-layer case with planar interfaces

In the case of a dipping refractor (Fig. 5.5(a)) the value of dip enters the travel-time equations as an additional unknown. The reciprocal of the gradient of the travel-time curve no longer represents the refractor velocity but a quantity known as the *apparent velocity* which is higher than the refractor velocity when recording along a profile line in the updip direction from the shot point and lower when recording downdip.

The conventional method of dealing with the possible presence of refractor dip is to *reverse* the refraction experiment by firing at each end of the profile line and recording seismic arrivals along the line from both shots. In the presence of a component of refractor dip along the profile direction, the *forward* and *reverse* travel time plots for refracted rays will differ in their gradients and intercept times, as shown in Fig. 5.5(b).

The general form of the equation for the travel-time t_n of a ray critically refracted in the nth dipping refractor (Fig. 5.6; Johnson 1976) is given by

$$t_n = \frac{x \sin\beta_1}{v_1} + \sum_{i=1}^{n-1} \frac{h_i(\cos\alpha_i + \cos\beta_i)}{v_i} \tag{5.8}$$

where h_i is the vertical thickness of the ith layer beneath the shot, v_i is the velocity of the ray in the ith layer, α_i is the angle with respect to the vertical made by the downgoing ray in the ith layer, β_i is the angle with respect to the vertical made by the upgoing ray in the ith layer, and x is the offset distance between source and detector.

Equation (5.8) is comparable with equation (5.7), the only differences being the replacement of θ by angles α and β that include a dip term. In the case of shooting downdip, for example (see Fig. 5.6), $\alpha_i = \theta_{in} - \gamma_i$ and $\beta_i = \theta_{in} + \gamma_i$, where γ_i is the dip of the ith layer and $\theta_{in} = \sin^{-1}(v_1/v_n)$ as before. Note that h is the vertical thickness rather than the perpendicular or true thickness of a layer (z).

As an example of the use of equation (5.8) in interpreting travel-time curves, consider the two-layer case illustrated in Fig. 5.5.

Shooting downdip, along the forward profile

$$\begin{aligned} t_2 &= \frac{x \sin\beta_1}{v_1} + \frac{h_1(\cos\alpha + \cos\beta)}{v_1} \\ &= \frac{x \sin(\theta_{12} + \gamma_1)}{v_1} + \frac{h_1 \cos(\theta_{12} - \gamma_1)}{v_1} \\ &\quad + \frac{h_1 \cos(\theta_{12} + \gamma_1)}{v_1} \\ &= \frac{x \sin(\theta_{12} + \gamma_1)}{v_1} + \frac{2h_1 \cos\theta_{12} \cos\gamma_1}{v_1} \\ &= \frac{x \sin(\theta_{12} + \gamma_1)}{v_1} + \frac{2z \cos\theta_{12}}{v_1} \end{aligned} \tag{5.9}$$

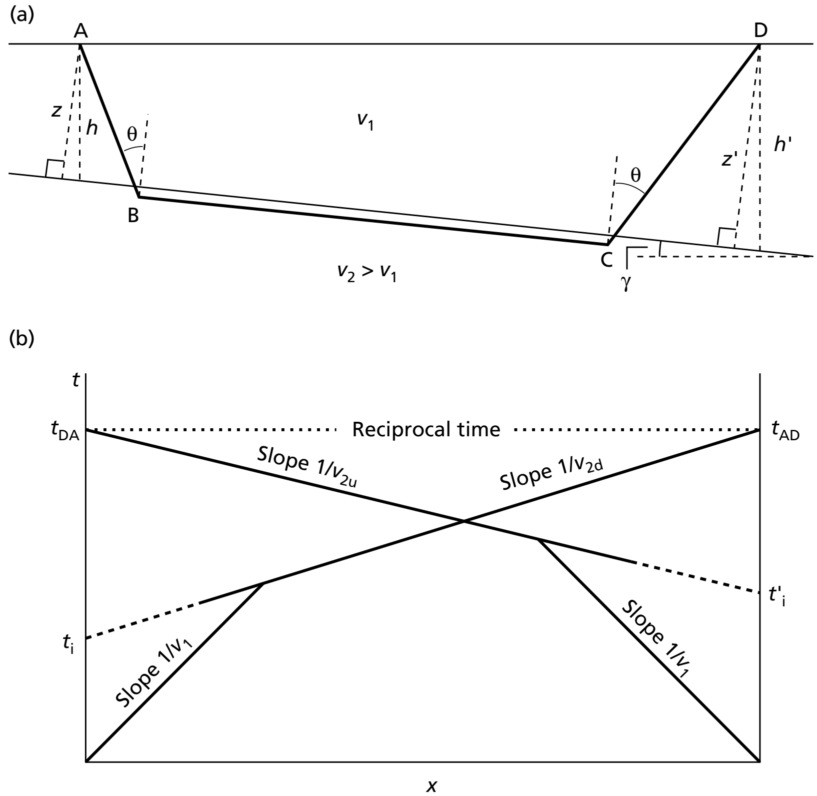

Fig. 5.5 (a) Ray-path geometry and (b) travel-time curves for head wave arrivals from a dipping refractor in the forward and reverse directions along a refraction profile line.

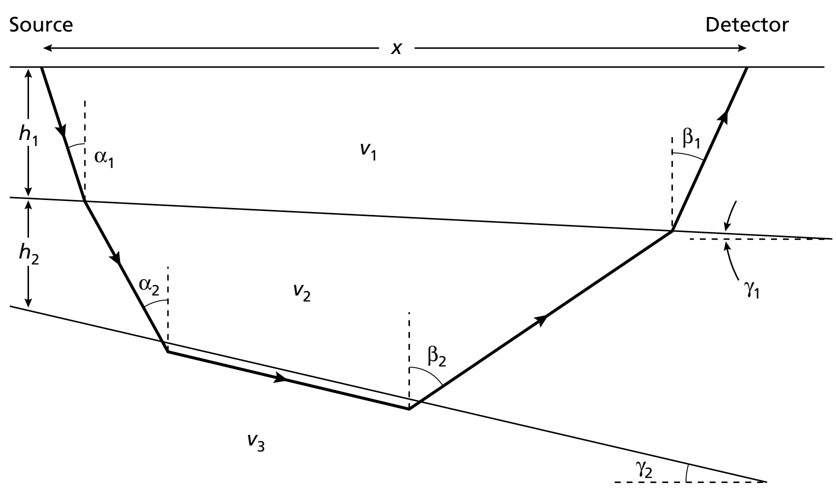

Fig. 5.6 Geometry of the refracted ray path through a multilayer, dipping model. (After Johnson 1976.)

where z is the perpendicular distance to the interface beneath the shot, and $\theta_{12} = \sin^{-1}(v_1/v_2)$.

Equation (5.9) defines a linear plot with a gradient of $\sin(\theta_{12} + \gamma_1)/v_1$ and an intercept time of $2z\cos\theta_{12}/v_1$.

Shooting updip, along the reverse profile

$$t_2' = \frac{x\sin(\theta_{12} - \gamma_1)}{v_1} + \frac{2z'\cos\theta_{12}}{v_1} \tag{5.10}$$

where z' is the perpendicular distance to the interface beneath the second shot.

The gradients of the travel-time curves of refracted arrivals along the forward and reverse profile lines yield the downdip and updip apparent velocities v_{2d} and v_{2u} respectively (Fig. 5.5(b)). From the forward direction

$$1/v_{2d} = \sin(\theta_{12} + \gamma_1)/v_1 \tag{5.11}$$

and from the reverse direction

$$1/v_{2u} = \sin(\theta_{12} - \gamma_1)/v_1 \tag{5.12}$$

Hence

$$\theta_{12} + \gamma_1 = \sin^{-1}(v_1/v_{2d})$$
$$\theta_{12} - \gamma_1 = \sin^{-1}(v_1/v_{2u})$$

Solving for θ and γ yields

$$\theta_{12} = \frac{1}{2}[\sin^{-1}(v_1/v_{2d}) + \sin^{-1}(v_1/v_{2u})]$$
$$\gamma_1 = \frac{1}{2}[\sin^{-1}(v_1/v_{2d}) - \sin^{-1}(v_1/v_{2u})]$$

Knowing v_1, from the gradient of the direct ray travel-time curve, and θ_{12}, the true refractor velocity may be derived using Snell's Law

$$v_2 = v_1/\sin\theta_{12}$$

The perpendicular distances z and z' to the interface under the two ends of the profile are obtained from the intercept times t_i and t_i' of the travel-time curves obtained in the forward and reverse directions

$$t_i = 2z\cos\theta_{12}/v_1$$
$$\therefore \quad z = v_1 t_i/2\cos\theta_{12}$$

and similarly

$$z' = v_1 t_i'/2\cos\theta_{12}$$

By using the computed refractor dip γ_1, the respective perpendicular depths z and z' can be converted into vertical depths h and h' using

$$h = z/\cos\gamma_1$$

and

$$h' = z'/\cos\gamma_1$$

Note that the travel time of a seismic phase from one end of a refraction profile line to the other (i.e. from shot point to shot point) should be the same whether measured in the forward or the reverse direction. Referring to Fig. 5.5(b), this means that t_{AD} should equal t_{DA}. Establishing that there is satisfactory agreement between these *reciprocal times* (or *end-to-end* times) is a useful means of checking that travel-time curves have been drawn correctly through a set of refracted ray arrival times derived from a reversed profile.

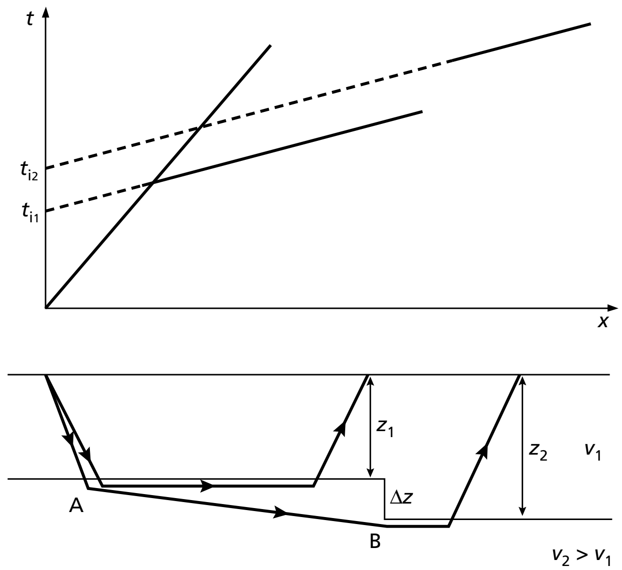

Fig. 5.7 Offset segments of the travel-time curve for refracted arrivals from opposite sides of a fault.

5.2.5 Faulted planar interfaces

The effect of a fault displacing a planar refractor is to offset the segments of the travel-time plot on opposite sides of the fault (see Fig. 5.7). There are thus two intercept times t_{i1} and t_{i2}, one associated with each of the travel-time curve segments, and the difference between these intercept times ΔT is a measure of the throw of the fault. For example, in the case of the faulted horizontal refractor shown in Fig. 5.7 the throw of the fault Δz is given by

$$\Delta T \approx \frac{\Delta z\cos\theta}{v_1}$$
$$\Delta z \approx \frac{\Delta T v_1}{\cos\theta} = \frac{\Delta T v_1 v_2}{(v_2^2 - v_1^2)^{1/2}}$$

Note that there is some approximation in this formulation, since the ray travelling to the downthrown side of the fault is not the critically refracted ray at A and involves diffraction at the base B of the fault step. However, the error will be negligible where the fault throw is small compared with the refractor depth.

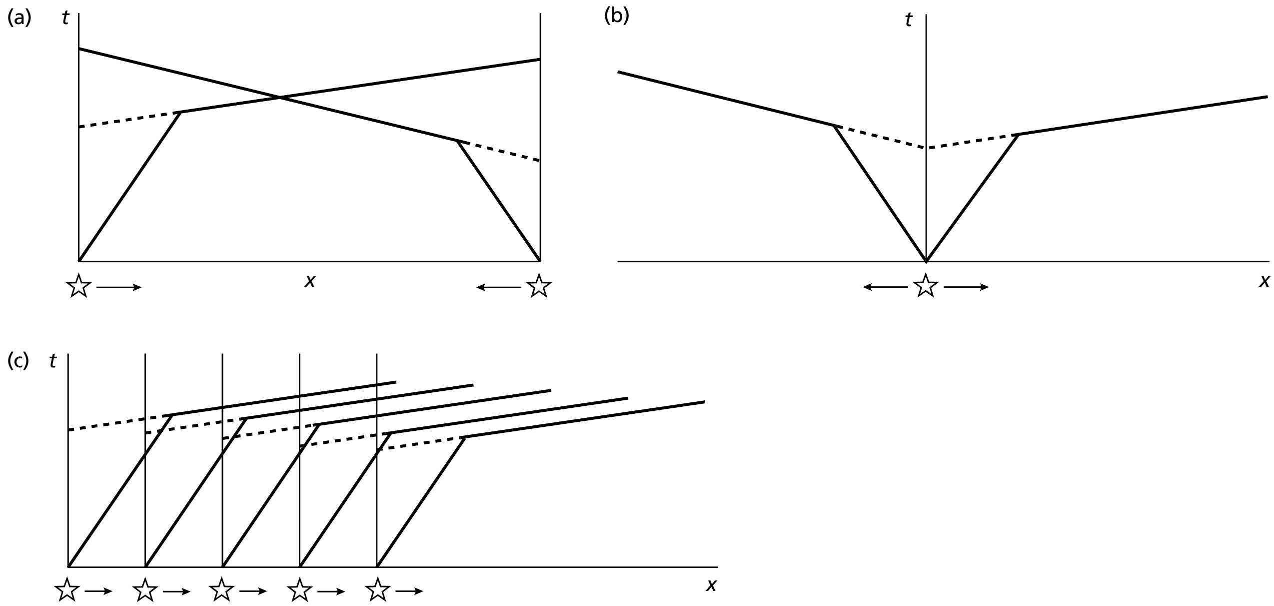

Fig. 5.8 Various types of profile geometry used in refraction surveying. (a) Conventional reversed profile with end shots. (b) Split-profile with central shot. (c) Single-ended profile with repeated shots.

5.3 Profile geometries for studying planar layer problems

The conventional field geometry for a refraction profile involves shooting at each end of the profile line and recording seismic arrivals along the line from both shots. As will be seen with reference to Fig. 5.5(a), only the central portion of the refractor (from B to C) is sampled by refracted rays detected along the line length. Interpreted depths to the refractor under the endpoints of a profile line, using equations given above, are thus not directly measured but are inferred on the basis of the refractor geometry over the shorter length of refractor sampled (BC). Where continuous cover of refractor geometry is required along a series of reversed profiles, individual profile lines should be arranged to overlap in order that all parts of the refractor are directly sampled by critically refracted rays.

In addition to the conventional reversed profile, illustrated schematically in Fig. 5.8(a), other methods of deriving full planar layer interpretations in the presence of dip include the *split-profile* method (Johnson 1976) and the *single-ended profile* method (Cunningham 1974). The split-profile method (Fig. 5.8(b)) involves recording outwards in both directions from a central shot point. Although the interpretation method differs in detail from that for a conventional reversed profile, it is based on the same general travel-time equation (5.8).

The single-ended profile method (Fig. 5.8(c)) was developed to derive interpretations of low-velocity surface layers represented by refracted arrivals in single-ended reflection spread data, for use in the calculation of static corrections. A simplified treatment is given below.

To obtain a value of refractor dip, estimates of apparent velocity are required in both the forward and reverse directions. The repeated forward shooting of the single-ended profile method enables an apparent velocity in the forward direction to be computed from the gradient of the travel-time curves. For the method of computing the apparent velocity in the reverse direction, consider two refracted ray paths from surface sources S_1 and S_2 to surface detectors D_1 and D_2, respectively (Fig. 5.9). The offset distance is x in both cases, the separation Δx of S_1 and S_2 being the same as that of D_1 and D_2.

Since D_1 is on the downdip side of S_1, the travel time of a refracted ray from S_1 to D_1 is given by equation (5.9), and omitting subscripts to θ and γ in this two-layer case,

$$t_1 = \frac{x\sin(\theta+\gamma)}{v_1} + \frac{2z_1\cos\theta}{v_1} \qquad (5.13)$$

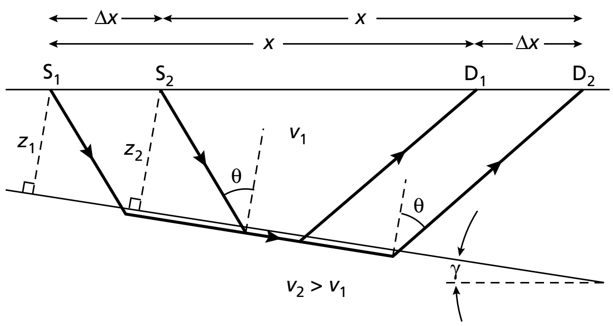

Fig. 5.9 Refraction interpretation using the single-ended profiling method. (After Cunningham 1974.)

and from S_2 to D_2 the travel time is given by

$$t_2 = \frac{x \sin(\theta + \gamma)}{v_1} + \frac{2z_2 \cos\theta}{v_1} \tag{5.14}$$

where z_1 and z_2 are the perpendicular depths to the refractor under shot points S_1 and S_2, respectively. Now,

$$\begin{aligned} z_2 - z_1 &= \Delta x \sin\gamma \\ \therefore z_2 &= z_1 + \Delta x \sin\gamma \end{aligned} \tag{5.15}$$

Substituting equation (5.15) in (5.14) and then subtracting equation (5.13) from (5.14) yields

$$\begin{aligned} t_2 - t_1 = \Delta t &= \frac{\Delta x}{v_1}(2\sin\gamma\cos\theta) \\ &= \frac{\Delta x \sin(\theta+\gamma)}{v_1} - \frac{\Delta x \sin(\theta-\gamma)}{v_1} \end{aligned}$$

Substituting equations (5.11) and (5.12) in the above equation and rearranging terms

$$\frac{\Delta t}{\Delta x} = \frac{1}{v_{2\mathrm{d}}} - \frac{1}{v_{2\mathrm{u}}}$$

where $v_{2\mathrm{u}}$ and $v_{2\mathrm{d}}$ are the updip and downdip apparent velocities, respectively. In the case considered $v_{2\mathrm{d}}$ is derived from the single-ended travel-time curves, hence $v_{2\mathrm{u}}$ can be calculated from the difference in travel time of refracted rays from adjacent shots recorded at the same offset distance x. With both apparent velocities calculated, interpretation proceeds by the standard methods for conventional reversed profiles discussed in Section 5.2.4.

5.4 Geometry of refracted ray paths: irregular (non-planar) interfaces

The assumption of planar refracting interfaces would often lead to unacceptable error or imprecision in the interpretation of refraction survey data. For example, a survey may be carried out to study the form of the concealed bedrock surface beneath a valley fill of alluvium or glacial drift. Such a surface is unlikely to be modelled adequately by a planar refractor. In such cases the constraint that refracting interfaces be interpreted as planar must be dropped and different interpretation methods must be employed.

The travel-time plot derived from a survey provides a first test of the prevailing refractor geometry. A layered sequence of planar refractors gives rise to a travel-time plot consisting of a series of straight-line segments, each segment representing a particular refracted phase and characterized by a particular gradient and intercept time. Irregular travel-time plots are an indication of irregular refractors (or of lateral velocity variation within individual layers—a complication not discussed here). Methods of interpreting irregular travel-time plots, to determine the non-planar refractor geometry that gives rise to them, are based on the concept of *delay time*.

5.4.1 Delay time

Consider a horizontal refractor separating upper and lower layers of velocity v_1 and v_2 ($>v_1$), respectively (Fig. 5.1). The travel time of a head wave arriving at an offset distance x is given (see equation (5.3)) by

$$t = \frac{x}{v_2} + t_{\mathrm{i}}$$

The intercept time t_{i} can be considered as composed of two delay times resulting from the presence of the top layer at each end of the ray path. Referring to Fig. 5.10(a), the *delay time* (or *time term*) δ_{t} is defined as the time difference between the slant path AB through the top layer and the time that would be required for a ray to travel along BC. The equation above clearly shows that the total travel time can be considered as the time a wave would take to travel the whole distance x at refractor velocity v_2, plus additional time t_{i} taken for the wave to travel down to the refractor at the shot point, and back up to the receiver. These two extra components of time are the *delay times* at the shot and receiver. Each delay time can be calculated in a similar way, referring to Fig. 5.10,

$$\begin{aligned}\delta_{\mathrm{t}} &= t_{\mathrm{AB}} - t_{\mathrm{BC}} \\ &= \frac{\mathrm{AB}}{v_1} - \frac{\mathrm{BC}}{v_2} \\ &= \frac{z}{v_1 \cos\theta} - \frac{z}{v_2}\tan\theta \\ &= \frac{z}{v_1 \cos\theta} - \frac{z\sin\theta}{v_1}\frac{\sin\theta}{\cos\theta} \\ &= \frac{z(1-\sin^2\theta)}{v_1\cos\theta} = \frac{z\cos\theta}{v_1} \\ &= \frac{z(v_2^2 - v_1^2)^{1/2}}{v_1 v_2}\end{aligned} \tag{5.16}$$

Solving equation (5.16) for the depth z to the refractor yields

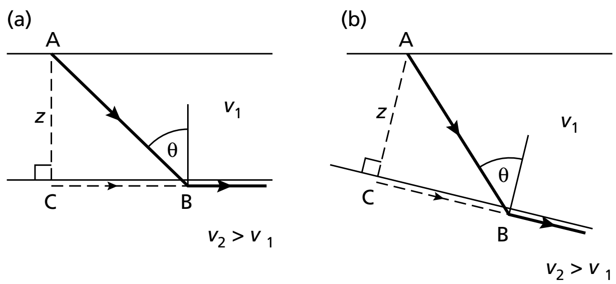

Fig. 5.10 The concept of delay time.

$$z = \delta_{\mathrm{t}} v_1 / \cos\theta = \delta_t v_1 v_2 / (v_2^2 - v_1^2)^{\frac{1}{2}} \tag{5.17}$$

Thus the delay time can be converted into a refractor depth if v_1 and v_2 are known.

The intercept time t_{i} in equation (5.3) can be partitioned into two delay times

$$t = x/v_2 + \delta_{\mathrm{ts}} + \delta_{\mathrm{td}} \tag{5.18}$$

where δ_{ts} and δ_{td} are the delay times at the shot end and detector end of the refracted ray path. Note that in this case of a horizontal refractor,

$$t = \frac{x}{v_2} + \frac{z\cos\theta}{v_1} + \frac{z\cos\theta}{v_1} = \frac{x}{v_2} + \frac{2z\cos\theta}{v_1}$$

This is the same result as derived earlier in equation (5.1), showing that the delay-time concept is implicit even in simple horizontal–lateral interpretation methods.

In the presence of refractor dip the delay time is similarly defined except that the geometry of triangle ABC rotates with the refractor. The delay time is again related to depth by equation (5.17), where z is now the refractor depth at A measured normal to the refractor surface. Using this definition of delay time, the travel time of a ray refracted along a dipping interface (see Fig. 5.11(a)) is given by

$$t = x'/v_2 + \delta_{\mathrm{ts}} + \delta_{\mathrm{td}} \tag{5.19}$$

where $\delta_{\mathrm{ts}} = t_{\mathrm{AB}} - t_{\mathrm{BC}}$ and $\delta_{\mathrm{td}} = t_{\mathrm{DE}} - t_{\mathrm{DF}}$.

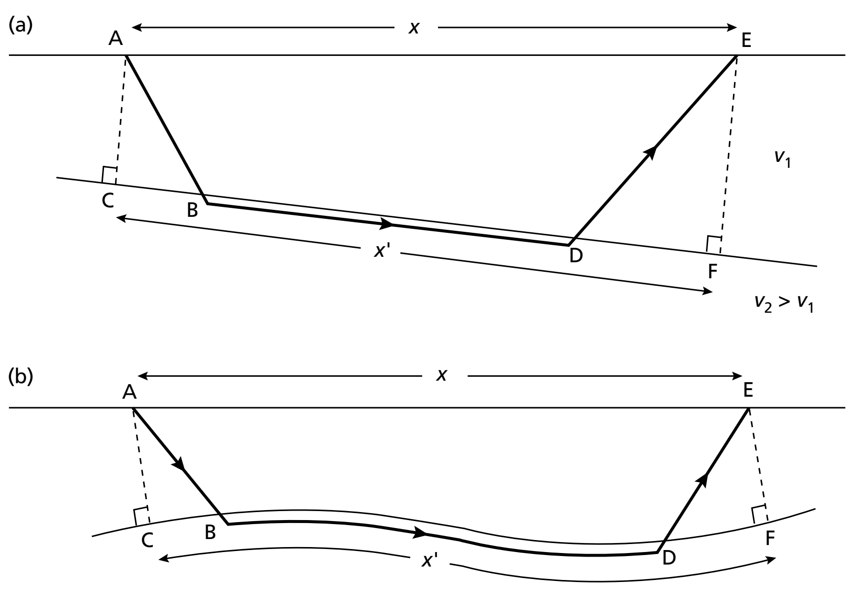

Fig. 5.11 Refracted ray paths associated with (a) a dipping and (b) an irregular refractor.

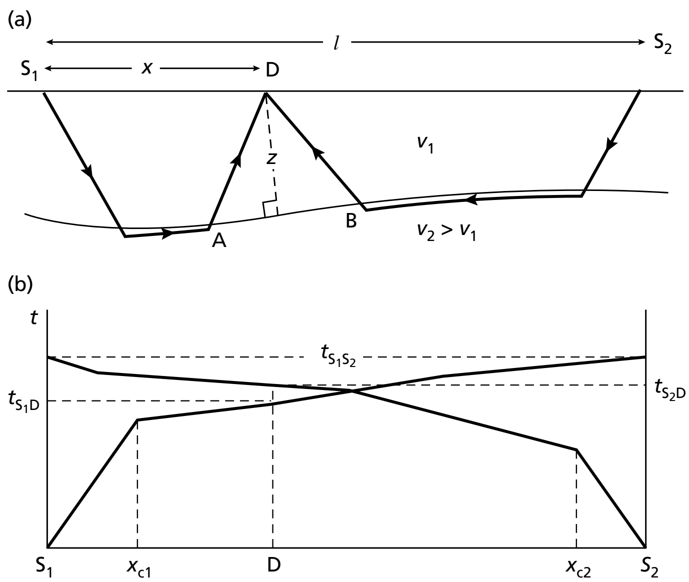

Fig. 5.12 The plus–minus method of refraction interpretation (Hagedoorn 1959). (a) Refracted ray paths from each end of a reversed seismic profile line to an intermediate detector position. (b) Travel-time curves in the forward and reverse directions.

For shallow dips, x' (unknown) is closely similar to the offset distance x (known), in which case equation (5.18) can be used in place of (5.19) and methods applicable to a horizontal refractor employed. This approximation is valid also in the case of an irregular refractor if the relief on the refractor is small in amplitude compared to the average refractor depth (Fig. 5.11(b)).

Delay times cannot be measured directly but occur in pairs in the travel-time equation for a refracted ray from a surface source to a surface detector. The *plus–minus method* of Hagedoorn (1959) provides a means of solving equation (5.18) to derive individual delay time values for the calculation of local depths to an irregular refractor.

5.4.2 The plus–minus interpretation method

Figure 5.12(a) illustrates a two-layer ground model with an irregular refracting interface. Selected ray paths are shown associated with a reversed refraction profile line of length l between end shot points S_1 and S_2. The travel time of a refracted ray travelling from one end of the line to the other is given by

$$t_{S_1S_2} = l/v_2 + \delta_{tS_1} + \delta_{tS_2} \tag{5.20}$$

where δ_{tS_1} and δ_{tS_2} are the delay times at the shot points. Note that $t_{S_1S_2}$ is the reciprocal time for this reversed profile (see Fig. 5.12(b)). For rays travelling to an intermediate detector position D from each end of the line, the travel times are, for the forward ray, from shot point S_1

$$t_{S_1D} = x/v_2 + \delta_{tS_1} + \delta_{tD} \tag{5.21}$$

for the reverse ray, from shot point S_2

$$t_{S_2D} = (l-x)/v_2 + \delta_{tS_2} + \delta_{tD} \tag{5.22}$$

where δ_{tD} is the delay time at the detector.

V_2 cannot be obtained directly from the irregular travel-time curve of refracted arrivals, but it can be estimated by means of Hagedoorn's *minus* term. This is obtained by taking the difference of equations (5.21) and (5.22)

$$\begin{aligned} t_{S_1D} - t_{S_2D} &= 2x/v_2 - l/v_2 + \delta_{tS_1} - \delta_{tS_2} \\ &= (2x-l)/v_2 + \delta_{tS_1} - \delta_{tS_2} \end{aligned}$$

This subtraction eliminates the variable (geophone-station dependent) delay time δ_{tD} from the above equation. Since the last two terms on the right-hand side of the equation are constant for a particular profile line, plotting the minus term $(t_{S_1D} - t_{S_2D})$ against the distance $(2x - l)$ yields a graph of slope $1/v_2$ from which v_2 may be derived. If the assumptions of the plus–minus method are valid, then the minus-time plot will be a straight line. Thus, this plot is a valuable quality control check for the interpretation method. Often it can be difficult to locate the crossover distances in real data, especially if the refracted arrivals line is irregular due to refractor topography. For minus-time points computed from arrival times which are not from the same refractor, the plot will curve away from a central straight section. Also, any lateral change of refractor velocity v_2 along the profile line will show up as a change of gradient in the minus term plot.

For the valid range of detectors determined from the minus-time plot, the delay times can now be calculated. Adding equations (5.21) and (5.22)

$$t_{S_1D} + t_{S_2D} = l/v_2 + \delta_{tS_1} + \delta_{tS_2} + 2\delta_{tD}$$

Substituting equation (5.20) in the above equation yields

$$t_{S_1D} + t_{S_2D} = t_{S_1S_2} + 2\delta_{tD}$$

Hence

$$\delta_{tD} = \frac{1}{2}\left(t_{S_1D} + t_{S_2D} - t_{S_1S_2}\right) \tag{5.23}$$

This delay time is the *plus* term of the plus–minus method and may be used to compute the perpendicular depth z to the underlying refractor at D using equation (5.17). v_2 is found from the minus-time plot and v_1 is computed from the slope of the direct ray travel-time plot (see Fig. 5.12(b)). Note that the value of all delay times depends on the *reciprocal time*. Errors in this time, which is recorded at maximum range along the profile, and often with the lowest signal-to-noise ratio, introduce a constant error into all delay times. Great care must be taken to check the errors in this value.

A plus term and, hence, a local refractor depth can be computed at all detector positions at which head wave arrivals are recognized from both ends of the profile line. In practice, this normally means the portion of the profile line between the crossover distances; that is, between x_{c1} and x_{c2} in Fig. 5.12(b).

Where a refractor is overlain by more than one layer, equation (5.17) cannot be used directly to derive a refractor depth from a delay time (or plus term). In such a case, either the thickness of each overlying layer is computed separately using refracted arrivals from the shallower interfaces, or an average overburden velocity is used in place of v_1 in equation (5.17) to achieve a depth conversion.

The plus–minus method is only applicable in the case of shallow refractor dips, generally being considered valid for dips of less than 10°. With steeper dips, x' becomes significantly different from the offset distance x. Further, there is an inherent smoothing of the interpreted refractor geometry in the plus–minus method.

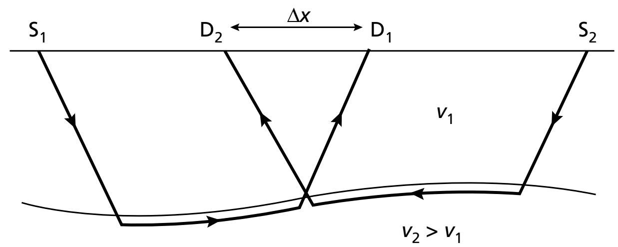

Fig. 5.13 The generalized reciprocal method of refraction interpretation (Palmer 1980).

When computing the plus term for each detector, the refractor is assumed to be planar between the points of emergence from the refractor of the forward and reverse rays, for example between A and B in Fig. 5.12(a) for rays arriving at detector D.

5.4.3 The generalized reciprocal method

This problem of smoothing is solved in the *generalized reciprocal method (GRM)* of refraction interpretation (Palmer 1980) by combining the forward and reverse rays which leave the refractor at approximately the same point and arrive at different detector positions separated by a distance Δx (see Fig. 5.13). The method uses a velocity analysis function t_v given by

$$t_v = \left(t_{S_1D_1} + t_{S_2D_2} - t_{S_1S_2}\right)/2 \tag{5.24}$$

the values being referred to the mid-point between each pair of detector positions D_1 and D_2. For the case where $D_1 = D_2 = D$ (i.e. $\Delta x = 0$), equation (5.24) reduces to a form similar to Hagedoorn's minus term (see above). The optimal value of Δx for a particular survey is that which produces the closest approach to a linear plot when the velocity analysis function t_v is plotted against distance along the profile line, and is derived by plotting curves for a range of possible Δx values. The overall interpretation method is more complex than the plus–minus method, but can deliver better velocity discrimination, greater lateral resolution and better depth estimates to boundaries. The method also demands denser data coverage than the plus–minus method. The principles of the method, its implementation and example datasets are clearly laid out in Palmer's book (Palmer 1980), but beyond the scope of this one.

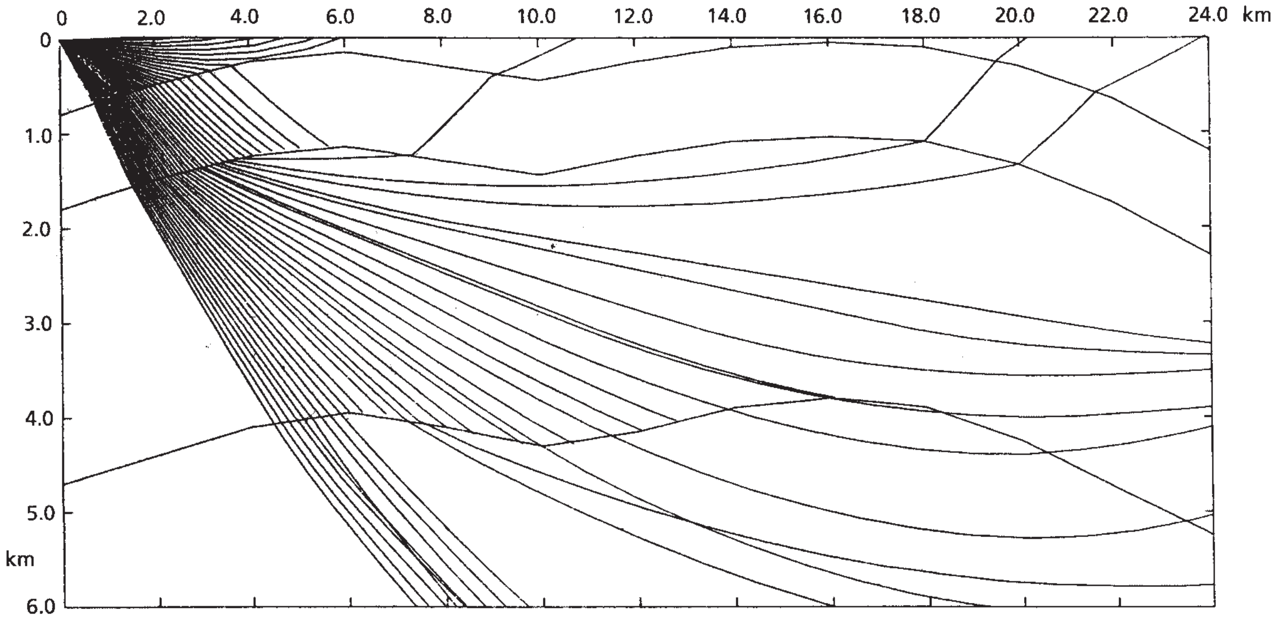

Fig. 5.14 Modelling of complex geology by ray-tracing in the case of a refraction profile between quarries in south Wales, UK. Refracted ray paths from Cornelly Quarry (located in Carboniferous Limestone) are modelled through a layered Palaeozoic sedimentary sequence overlying an irregular Precambrian basement surface at a depth of about 5 km. This model accounts for the measured travel times of refracted arrivals observed along the profile. (From Bayerly & Brooks 1980.)

5.5 Construction of wavefronts and ray-tracing

Given the travel-time plots in the forward and reverse directions along a profile line it is possible to reconstruct the configuration of successive wavefronts in the subsurface and thereby derive, graphically, the form of refracting interfaces. This *wavefront method* (Thornburgh 1930) represents one of the earliest refraction interpretation methods but is no longer widely used.

With the massive expansion in the speed and power of digital computers, and their wide availability, an increasingly important method of refraction interpretation is a modelling technique known as *ray-tracing* (Cerveny *et al.* 1974). In this method structural models are postulated and the travel-times of refracted (and reflected) rays through these models are calculated by computer for comparison with observed travel-times. The model is then adjusted iteratively until the calculated and observed travel-times are in acceptable agreement. This method is especially useful in the case of complex subsurface structures that are difficult to treat analytically. An example of a ray-tracing interpretation is illustrated in Fig. 5.14. The ray-tracing method is particularly valuable in coping with such complexities as horizontal or vertical velocity gradients within layers, highly irregular or steeply dipping refractor interfaces and discontinuous layers.

5.6 The hidden and blind layer problems

It is possible for layers to exist in the Earth, yet not produce any refracted first-arrival waves. In this case the layers will be undetectable in a simple first arrival refraction survey. The observed data could be interpreted using the methods discussed above and yield a self-consistent, but erroneous, solution. For this reason, the possibility of undetected layers should always be considered. In practice, there are two different types of problem. In order to be detected in a first arrival refraction survey, a layer must (a) be underlain by a layer of higher velocity so that head waves are produced, and (b) have a thickness and velocity such that the head waves become first arrivals at some range.

A *hidden layer* is a layer which, whilst producing head waves, does not give rise to first arrivals. Rays travelling to deeper levels arrive before those critically refracted at the top of the layer in question (Fig. 5.15(a)). This may

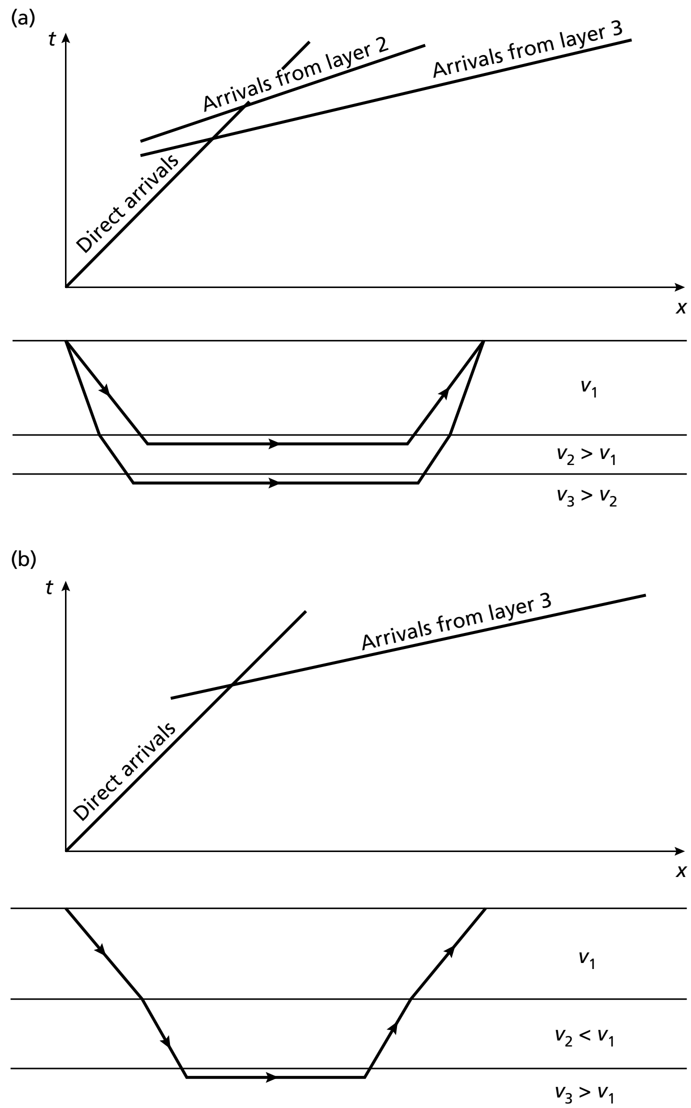

Fig. 5.15 The undetected layer problem in refraction seismology. (a) A hidden layer: a thin layer that does not give rise to first arrivals. (b) A blind layer: a layer of low velocity that does not generate head waves.

result from the thinness of the layer, or from the closeness of its velocity to that of the overlying layer. In such a case, a method of survey involving recognition of only first arrivals will fail to detect the layer. It is good practice to examine the seismic traces for possible arrivals occurring behind the first arrivals. These should then be examined to ensure they are compatible with the structural model derived from the first arrivals.

A *blind layer* presents a more insidious problem, resulting from a low-velocity layer, as illustrated in Fig. 5.15(b). Rays cannot be critically refracted at the top of such a layer and the layer will therefore not give rise to head waves. Hence, a low-velocity layer cannot be detected by refraction surveying, although the top of the low-velocity layer gives rise to wide-angle reflections that may be detected as later arrivals during a refraction survey.

In the presence of a low-velocity layer, the interpretation of travel-time curves leads to an overestimation of the depth to underlying interfaces. Low-velocity layers are a hazard in all types of refraction seismology. On a small scale, a peat layer in muds and sands above bedrock may escape detection, leading to a false estimation of foundation conditions and rockhead depths beneath a construction site; on a much larger scale, low-velocity zones of regional extent are known to exist within the continental crust and may escape detection in crustal seismic experiments.

5.7 Refraction in layers of continuous velocity change

In some geological situations, velocity varies gradually as a function of depth rather than discontinuously at discrete interfaces of lithological change. In thick clastic sequences, for example, especially clay sequences, velocity increases downwards due to the progressive compaction effects associated with increasing depth of burial. A seismic ray propagating through a layer of gradual velocity change is continuously refracted to follow a curved ray path. For example, in the special case where velocity increases linearly with depth, the seismic ray paths describe arcs of circles. The deepest point reached by a ray travelling on a curved path is known as its *turning point*.

In such cases of continuous velocity change with depth, the travel-time plot for refracted rays that return to the surface along curved ray paths is itself curved, and the geometrical form of the curve may be analysed to derive information on the distribution of velocity as a function of depth (see e.g. Dobrin & Savit 1988).

Velocity increase with depth may be significant in thick surface layers of clay due to progressive compaction and dewatering, but may also be significant in deeply buried layers. Refracted arrivals from such buried layers are not true head waves since the associated rays do not travel along the top surface of the layer but along a curved path in the layer with a turning point at some depth below the interface. Such refracted waves are referred to as *diving waves* (Cerveny & Ravindra 1971). Methods of interpreting refraction data in terms of diving waves are generally complex, but include ray-tracing techniques. Indeed, some ray-tracing programmes require velocity gradients to be introduced into all layers of an interpretation model in order to generate diving waves rather than true head waves.

5.8 Methodology of refraction profiling

Many of the basic principles of refraction surveying have been covered in the preceding sections but in this section several aspects of the design of refraction profile lines are brought together in relation to the particular objectives of a refraction survey.

5.8.1 Field survey arrangements

Although the same principles apply to all scales of refraction profiling, the logistic problems of implementing a profile line increase as the required line length increases. Further, the problems of surveying on land are quite different from those encountered at sea. A consequence of these logistic differences is a very wide variety of survey arrangements for the implementation of refraction profile lines and these differences are illustrated by three examples.

For a small-scale refraction survey of a construction site to locate the water table or rockhead (both of which surfaces are generally good refractors), recordings out to an offset distance of about 100 m normally suffice. Geophones are connected via a multicore cable to a portable 24- or 48-channel seismic recorder. A simple weight-dropping device (even a sledge hammer impacted on to a steel base plate) provides sufficient energy to traverse the short recording range. The dominant frequency of such a source exceeds 100 Hz and the required accuracy of seismic travel times is about 0.5 ms. Such a survey can be easily accomplished by two operators.

The logistic difficulties associated with the cable connection between a detector spread and a recording unit normally limit conventional refraction surveys to maximum shot–detector offsets of about 1 km and, hence, to depths of investigation of a few hundred metres. For larger scale refraction surveys it is necessary to dispense with a cable connection. At sea, such surveys can be carried out by a single vessel in conjunction with free-floating radio-transmitting sonobuoys (Fig. 5.16). Having deployed the sonobuoys, the vessel proceeds along the profile line repeatedly firing explosive charges or an air-gun array. Seismic signals travelling back to the surface through the water layer are detected by a hydrophone suspended beneath each sonobuoy, amplified and transmitted back to the survey vessel where they are recorded along with the shot instant. By this means, refraction lines up to a few tens of kilometres may be implemented.

For large-scale marine surveys, ocean bottom seismographs (OBSs) are deployed on the sea bed. These contain a digital recorder together with a high-precision clock unit to provide an accurate time base for the seismic recordings. Such instruments may be deployed for periods of up to a few days at a time. For the purposes of recovery, the OBSs are 'popped-up' to the surface by remotely triggering a release mechanism. Sea-bed recording systems provide a better signal-to-noise ratio than hydrophones suspended in the water column and, in deep water, recording on the sea bed allows much better definition of shallow structures. In this type of survey the dominant frequency is typically in the range

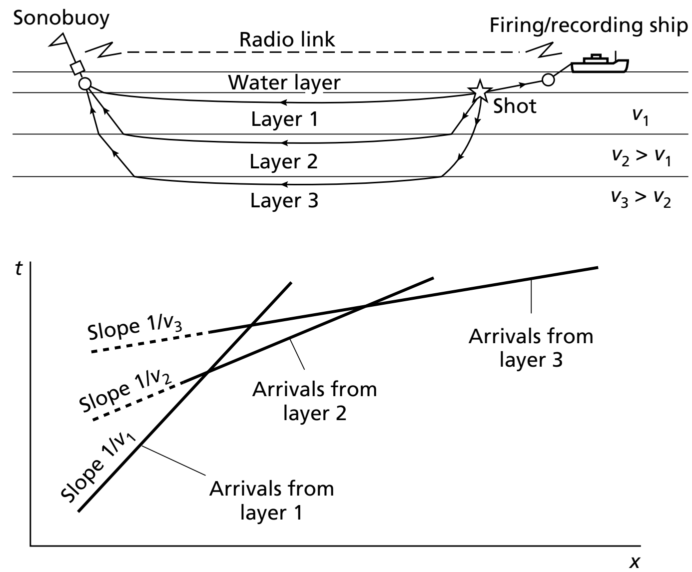

Fig. 5.16 Single-ship seismic refraction profiling.

10–50 Hz and travel times need to be known to about 10 ms.

A large-scale seismic refraction line on land to investigate deep crustal structure is typically 250–300 km long. Seismic events need to be recorded at a series of independently operated recording stations all receiving a standard time signal to provide a common time base for the recordings. Usually this is provided by the signal from the global positioning system (GPS) satellite system. Very large energy sources, such as military depth charges (detonated at sea or in a lake) or large quarry blasts, are required in order that sufficient energy is transmitted over the length of the profile line. The dominant frequency of such sources is less than 10 Hz and the required accuracy of seismic travel times is about 50 ms. Such an experiment requires the active involvement of a large and well-coordinated field crew.

Along extended refraction lines, wide-angle reflection events are often detected together with the refracted phases. These provide an additional source of information on subsurface structure. Wide-angle reflection events are sometimes the most obvious arrivals and may represent the primary interest (e.g. Brooks *et al.* 1984). Surveys specifically designed for the joint study of refracted and wide-angle reflection events are often referred to as *wide-angle surveys*.

5.8.2 Recording scheme

For complete mapping of refractors beneath a seismic line it is important to arrange that head wave arrivals

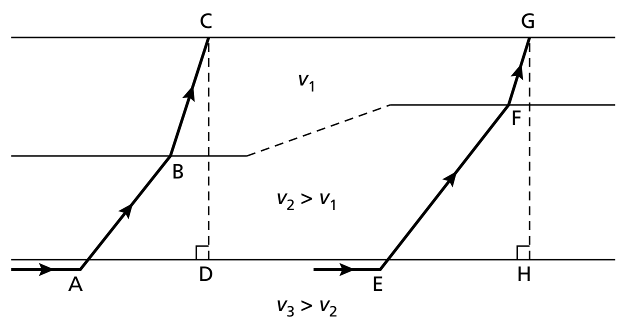

Fig. 5.17 Variation in the travel time of a head wave associated with variation in the thickness of a surface layer.

from all refractors of interest are obtained over the same portion of line. The importance of this can be seen by reference to Fig. 5.17 where it is shown that a change in thickness of a surface low-velocity layer would cause a change in the delay time associated with arrivals from a deeper refractor and may be erroneously interpreted as a change in refractor depth. The actual geometry of the shallow refractor should be mapped by means of shorter reversed profiles along the length of the main profile. These are designed to ensure that head waves from the shallow refractor are recorded at positions where the depth to the basal refractor is required. Knowledge of the disposition of the shallow refractor derived from the shorter profiles would then allow correction of travel times of arrivals from the deeper refractor.

The general design requirement is the formulation of an overall observational scheme as illustrated in

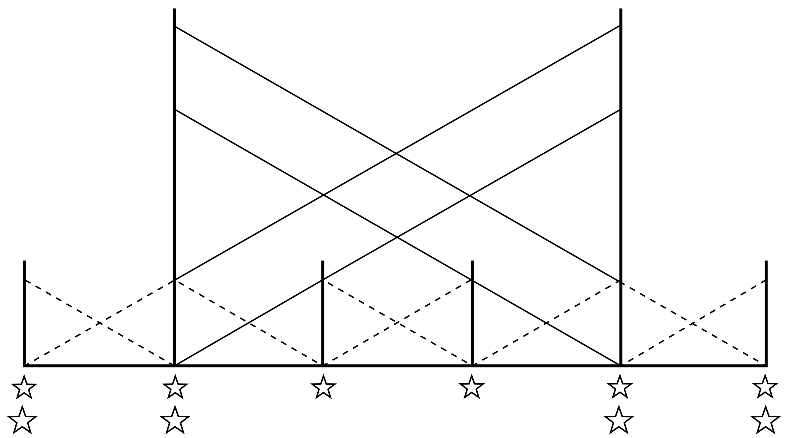

Fig. 5.18 A possible observational scheme to obtain shallow and deeper refraction coverage along a survey line. The inclined lines indicate the range of coverage from the individual shots shown.

Fig. 5.18. Such a scheme might include off-end shots into individual reversed profile lines, since off-end shots extend the length of refractor traversed by recorded head waves and provide insight into the structural causes of any observed complexities in the travel-time curves. Selection of detector spacing along the individual profile lines is determined by the required detail of the refractor geometry, the sampling interval of interpretation points on the refractor being approximately equal to the detector spacing. Thus, the horizontal resolution of the method is equivalent to the detector spacing.

It is often the case that there are insufficient detectors available to cover the full length of the profile with the desired detector spacing. In this case the procedure is to deploy the detectors to cover one segment of the line at the required spacing, then to fire shots at all shot points. The detectors are then moved to another segment of the line and all shot points fired again. The process can be repeated until full data are compiled for the complete profile. At the price of repeating the shots, a profile can thus be recorded of any length with a limited supply of equipment. The same principle is equally applicable to shallow penetration, to detailed refraction surveys for engineering, to environmental and hydrological applications, and to crustal studies.

5.8.3 Weathering and elevation corrections

The type of observational scheme illustrated in Fig. 5.18 is often implemented for the specific purpose of mapping the surface zone of weathering and associated low velocity across the length of a longer profile designed to investigate deeper structure. The velocity and thickness of the weathered layer are highly variable laterally and travel times of rays from underlying refractors need to be corrected for the variable delay introduced by the layer. This weathering correction is directly analogous to that applied in reflection seismology (see Section 4.6). The weathering correction is particularly important in shallow refraction surveying where the size of the correction is often a substantial percentage of the overall travel time of a refracted ray. In such cases, failure to apply an accurate weathering correction can lead to major error in interpreted depths to shallow refractors.

A weathering correction is applied by effectively replacing the weathered layer of velocity v_w with material of velocity v_1 equal to the velocity of the underlying layer. For a ray critically refracted along the top of the layer immediately underlying the weathered layer, the weathering correction is simply the sum of the delay times at the shot and detector ends of the ray path. Application of this correction replaces the refracted ray path by a direct path from shot to detector in a layer of velocity v_1. For rays from a deeper refractor a different correction is required. Referring to Fig. 5.19, this correction effectively replaces ray path ABCD by ray path AD. For a ray critically refracted in the nth layer the weathering correction t_w is given by

$$t_w = -(z_s + z_d) \times \left\{ (v_n^2 - v_1^2)^{1/2} \big/ v_1 v_n - (v_n^2 - v_w^2)^{1/2} \big/ v_w v_n \right\}$$

where z_s and z_d are the thicknesses of the weathered layer beneath the shot and detector respectively, and v_n is the velocity in the nth layer.

In addition to the weathering correction, a correction is also needed to remove the effect of differences in elevation of individual shots and detectors, and an elevation correction is therefore applied to reduce travel times to a

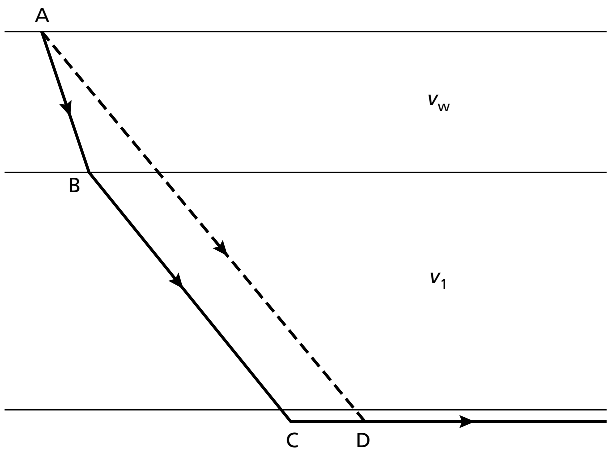

Fig. 5.19 The principle of the weathering correction in refraction seismology.

common datum plane. The elevation correction t_e for rays critically refracted in the nth layer is given by

$$t_e = -(h_s + h_d)\left\{(v_n^2 - v_1^2)^{1/2} \big/ v_1 v_n\right\}$$

where h_s and h_d are the heights above datum of the shot point and detector location respectively. It is worth noting that these corrections are more complex than those used for seismic reflection surveys. The difference arises since the assumption of vertical ray paths through the weathered layer used in the reflection case cannot be maintained.

In shallow water marine refraction surveying the water layer is conventionally treated as a weathered layer and a correction applied to replace the water layer by material of velocity equal to the velocity of the sea bed.

5.8.4 Display of refraction seismograms

In small-scale refraction surveys the individual seismograms are conventionally plotted out in their true time relationships in a format similar to that employed to display seismic traces from land reflection spreads (see Fig. 4.8). From such displays, arrival times of refracted waves may be picked and, after suitable correction, used to make the time–distance plots that form the basis of refraction interpretation.

Interpretation of large-scale refraction surveys is often as much concerned with later arriving phases, such as wide-angle reflections or S-wave arrivals, as with first arrivals. To aid recognition of weak coherent phases, the individual seismograms are compiled into an overall record section on which the various seismic phases can be correlated from seismogram to seismogram. The optimal type of display is achieved using a *reduced time* scale in which any event at time t and offset distance x is plotted at the reduced time T where

$$T = t - x/v_R$$

and v_R is a scaling factor known as the *reduction velocity*. Thus, for example, a seismic arrival from deep in the Earth's crust with an overall travel time of 30 s to an offset distance of 150 km would, with a reduction velocity of 6 km s^{-1}, have a reduced time of 5 s.

Plotting in reduced time has the effect of progressively reducing travel-time as a function of offset and, therefore, rotating the associated time–distance curves towards the horizontal. For example, a time–distance curve with a reciprocal slope of 6 km s^{-1} on a t–x graph would plot as a horizontal line on a T–x graph using a reduction velocity of 6 km s^{-1}. By appropriate choice of reduction velocity, seismic arrivals from a particular refractor of interest can be arranged to plot about a horizontal datum, so that relief on the refractor will show up directly as departures of the arrivals from a horizontal line. The use of reduced time also enables the display of complete seismograms with an expanded time scale appropriate for the analysis of later arriving phases. An example of a record section from a crustal seismic experiment, plotted in reduced time, is illustrated in Fig. 5.20.

5.9 Other methods of refraction surveying

Although the vast bulk of refraction surveying is carried out along profile lines, other spatial arrangements of shots and detectors may be used for particular purposes. Such arrangements include *fan-shooting* and irregularly distributed shots and recorders as used in the *time term* method.

Fan-shooting (Fig. 5.21) is a convenient method of accurately delineating a subsurface zone of anomalous velocity whose approximate position and size are already known. Detectors are distributed around a segment of arc approximately centred on one or more shot points, and travel-times of refracted rays are measured to each detector. Through a homogeneous medium the travel-times to detectors would be linearly related to range, but

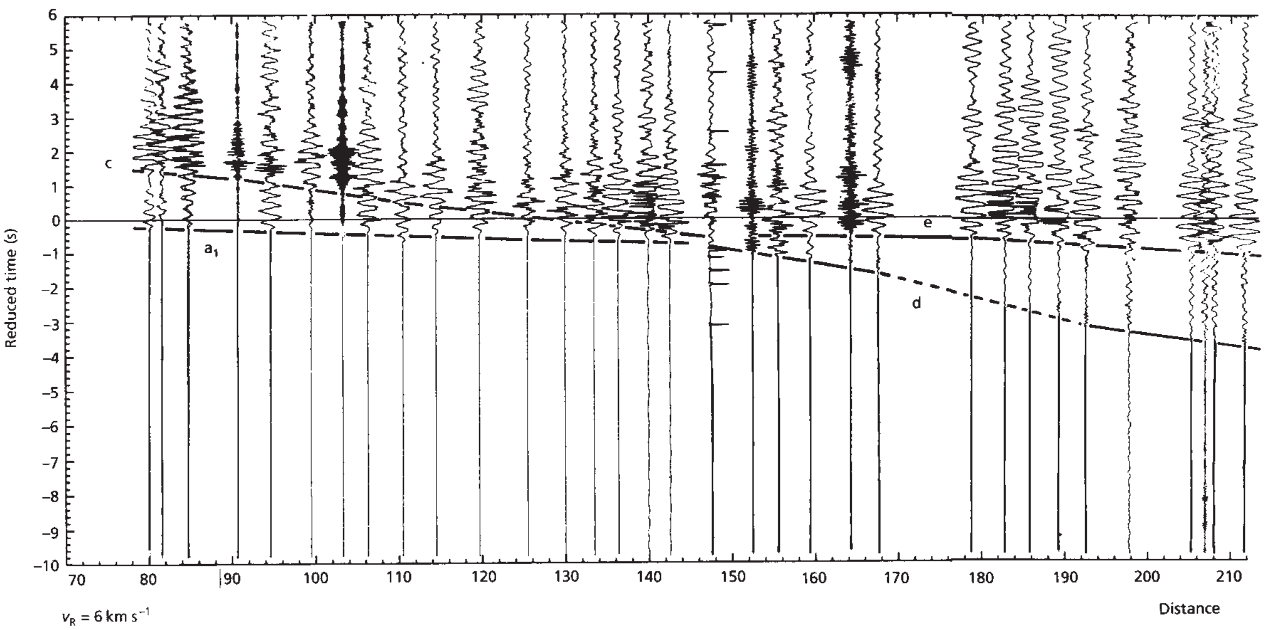

Fig. 5.20 Part of a time section from a large-scale refraction profile, plotted in reduced time using a reduction velocity of 6 km s^{-1}. The section was derived from the LISPB lithospheric seismic profile across Britain established in 1974. Phase a_1: head wave arrivals from a shallow crustal refractor with a velocity of about 6.3 km s^{-1}; phases c and e: wide-angle reflections from lower crustal interfaces: phase d: head wave arrivals from the uppermost mantle (the P_n phase of earthquake seismology). (From Bamford *et al.* 1978.)

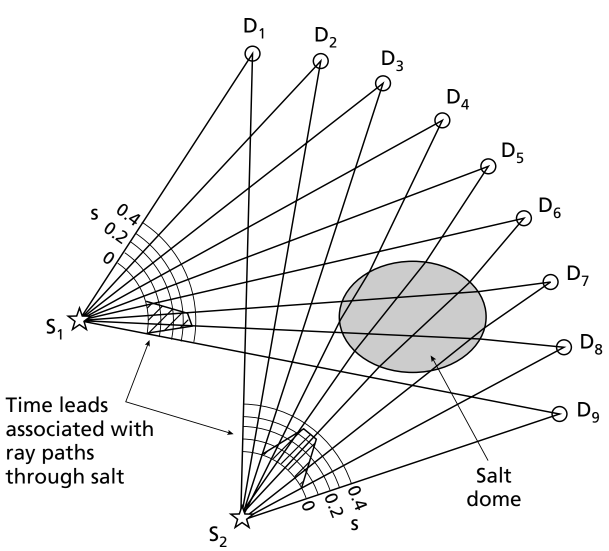

Fig. 5.21 Fan-shooting for the detection of localized zones of anomalous velocity.

any ray path which encounters an anomalous velocity zone will be subject to a time lead or time lag depending upon the velocity of the zone relative to the velocity of the surrounding medium. Localized anomalous zones capable of detection and delineation by fan-shooting include salt domes, buried valleys and backfilled mine shafts.

An irregular, areal distribution of shots and detectors (Fig. 5.22(a)) represents a completely generalized approach to refraction surveying and facilitates mapping of the three-dimensional geometry of a subsurface refractor using the *time term method* of interpretation (Willmore & Bancroft 1960, Berry & West 1966). Rather than being an intrinsic aspect of the survey design, however, an areal distribution of shot points and recording sites may result simply from an opportunistic approach to refraction surveying in which freely available sources of seismic energy such as quarry blasts are used to derive subsurface information from seismic recordings.

The *time term method* uses the form of the travel-time equation containing delay times (equation (5.18)) and is subject to the same underlying assumptions as other interpretation methods using delay times. However, in the time term method a statistical approach is adopted to deal with a redundancy of data inherent in the method and to derive the best estimate of the interpretation parameters. Introducing an error term into the travel-time equation

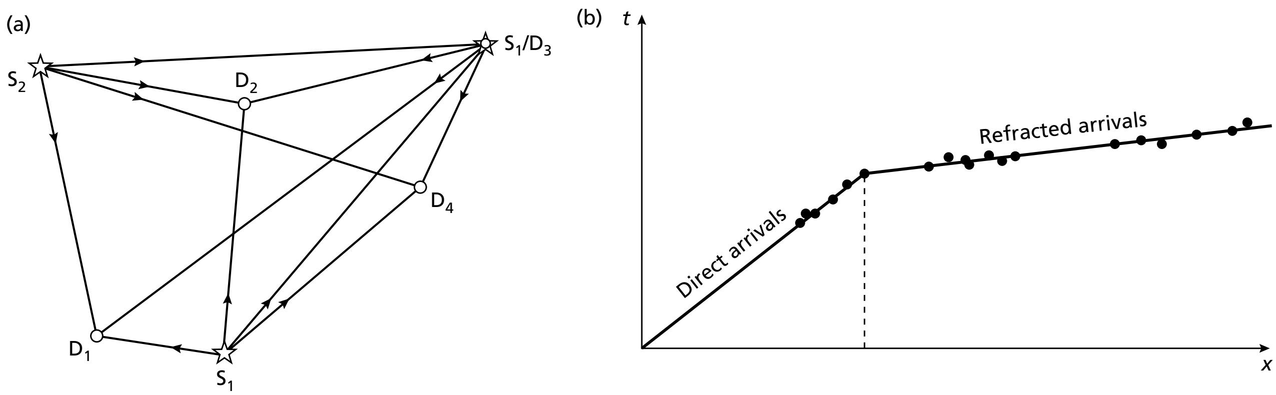

Fig. 5.22 (a) An example of the type of network of shots and detectors from which the travel times of refracted arrivals can be used in a time term analysis of the underlying refractor geometry. (b) The plot of travel time as a function of distance identifies the set of refracted arrivals that may be used in the analysis.

$$t_{ij} = x_{ij}/v + \delta_{ti} + \delta_{tj} + \varepsilon_{ij}$$

where t_{ij} is the travel time of head waves from the ith site to the jth site, x_{ij} is the offset distance between site i and site j, δ_{ti} and δ_{tj} are the delay times (time terms), v is the refractor velocity (assumed constant), and ε_{ij} is an error term associated with the measurement of t_{ij}.

If there are n sites there can be up to $n(n-1)$ observational linear equations of the above type, representing the situation of a shot and detector at each site and all sites sufficiently far apart for the observation of head waves from the underlying refractor. In practice there will be fewer observational equations than this because, normally, only a few of the sites are shot points and head wave arrivals are not recognized along every shot–detector path (Fig. 5.22(b)). There are $(n+1)$ unknowns, namely the individual delay times at the n sites and the refractor velocity v.

If the number m of observational equations equals the number of unknowns, the equations can be solved to derive the unknown quantities, although it is necessary either that at least one shot and detector position should coincide or that the delay time should be known at one site. In fact, with the time term approach to refraction surveying it is normally arranged for m to well exceed $(n+1)$, and for several shot and detector positions to be interchanged. The resulting overdetermined set of equations is solved by deriving values for the individual delay times and refractor velocity that minimize the sum of squares of the errors ε_{ij}. Delay times can then be converted into local refractor depths using the same procedure as in the plus–minus method described earlier.

5.10 Seismic tomography

Although fan-shooting involves surface shots and recorders, the method may be regarded as the historical precursor of an important group of modern exploration methods using shots and detectors located in boreholes. In these methods, known as *seismic tomography*, subsurface zones are systematically investigated by transmitting very large numbers of seismic rays through them. An example is cross-hole seismics (see e.g. Wong *et al*. 1987), in which shots generated at several depths down a borehole are recorded by detector arrays in an adjacent borehole to study variations in the seismic wave transmission through the intervening section of ground. A simple example is shown in Fig. 5.23, where only a limited subset of ray paths are shown.

The volume of ground under investigation is modelled as divided into cubic elements. The seismic sources and receivers are arranged so that multiple seismic rays pass through each element of that volume. If the geological unit under investigation is a near-horizontal bed, then the sources, receivers and volume elements lie in a single horizontal plane and the geometry is directly comparable to the cross-borehole situation. An example of this geometry is the investigation of coal seams prior to long-wall mining techniques. Here the sources and receivers are arranged in the tunnels driven to give access to the seam.

It is theoretically straightforward to develop the method to investigate 3D velocity structures. This is done for medical imaging such as CAT scanning, where X-rays are directed though the investigated volume by moving the source and receiver freely around the

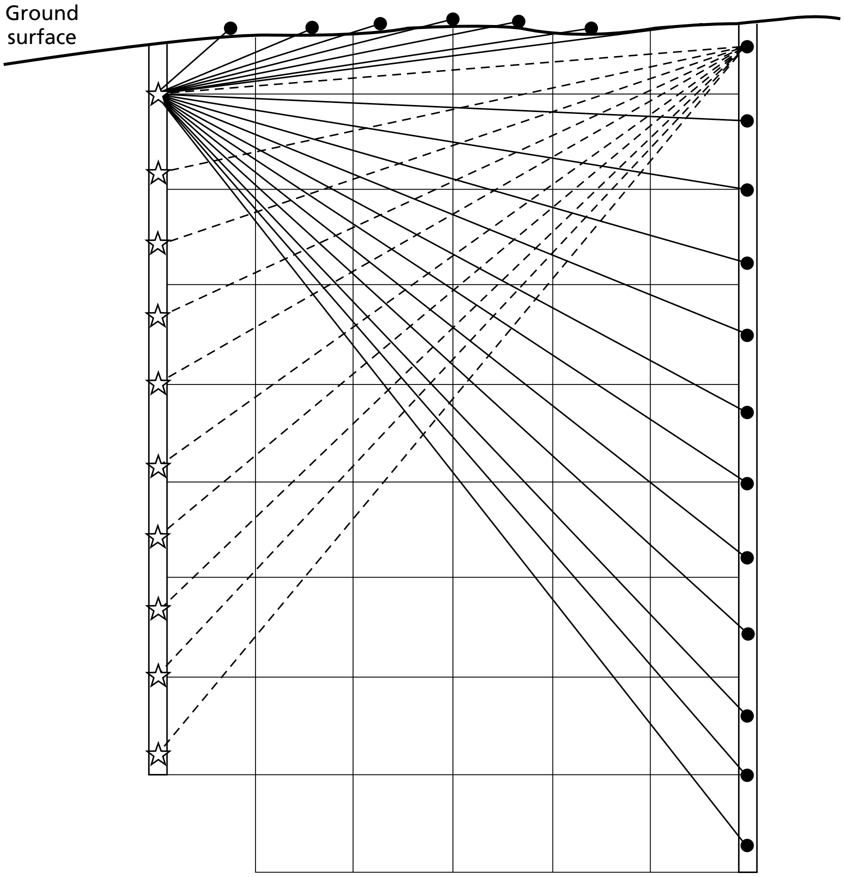

Fig. 5.23 Idealized observation scheme for a simple cross-hole seismic transmission tomography survey. Dots mark receivers, stars mark sources. For clarity, only the ray paths from one source to all receivers (solid lines), and all sources to one receiver (dashed lines) are shown. Also shown is the regular grid of elements for which velocity values are derived.

perimeter of the volume. In the geological case the difficulty lies in getting access to place sources and receivers at locations distributed uniformly around the volume under investigation. Multiple vertical boreholes merely allow the collection of a number of vertical 2D sections as shown in Fig. 5.23.

The total travel-times for each ray are the basic data used for interpretation. Each cubic element is assigned an initial seismic velocity. Assuming a linear ray path from source and receiver, the time spent by each ray in each element can be calculated. The velocity assigned to each individual element can then be adjusted so that the errors between the observed travel-times and the calculated ones are minimized. A more sophisticated approach is to include in the solution the effect of refraction of the seismic wave as it passes between volume elements of different velocity. Such a solution has more variable parameters and requires a dense pattern of intersecting ray paths within the irradiated section. Note that the calculation of the true ray path is very difficult. It cannot be found by applying Snell's Law at the element boundaries, since these boundaries have no physical reality. Common methods of solution of the resulting equations are the *algebraic reconstruction technique* (ART) and the *simultaneous reconstruction technique* (SIRT). The details of these techniques are beyond the scope of this book, but are well described by Ivansson (1986).

Use of high-frequency sources permits accurate travel-time determination and consequent high-resolution imaging of the velocity structure. This is necessary since a change in velocity in any one element only has a very small effect on the total travel-time for the ray path. Less commonly, parameters other than the P-wave travel-times can be analysed. Particular examples would be the S-wave travel-times, and the attenuation of the seismic wave. The above discussion has only considered transmission tomography, where the ray path is the simple minimum travel-time path from source to receiver. With additional complications, the same basic approach can be used with more complex ray paths. Reflection tomography involves the application of tomographic principles to reflected seismic waves. While it is considerably more complex than conventional seismic reflection processing, in areas of complex structure, particularly with large velocity variations, it can produce greatly improved seismic images.

The information derived from seismic tomography may be used to predict spatial variations in, for example, lithology, pore fluids, or rock fracturing, and the method is therefore of potential value in a wide range of exploration and engineering applications. As with many geophysical methods, it can also be applied on a variety of spatial scales, from ranges of hundreds of metres, down to engineering or archaeological investigations of single columns in ancient buildings (Cardarelli & de Nardis 2001).

5.11 Applications of seismic refraction surveying

Exploration using refraction methods covers a very wide range of applications. Refraction surveys can provide estimates of the elastic constants of local rock types, which have important engineering applications: use of special sources and geophones allows the separate recording of shear wave arrivals, and the combination of P- and S-wave velocity information enables calculation of Poisson's ratio (Section 3.3.1). If an estimate of density is available, the bulk modulus and shear modulus can also be calculated from P- and S-wave velocities. Such estimates of the elastic constants, based on the propagation of seismic waves, are referred to as dynamic, in contrast to the static estimates derived from load-testing of rock samples in the laboratory. Dynamic estimates tend to yield slightly higher values than loading tests.

5.11.1 Engineering and environmental surveys

On the local scale, refraction surveys are widely used in foundation studies on construction sites to derive estimates of depth to rockhead beneath a cover of superficial material. Use of the plus–minus method or the generalized reciprocal method (Section 5.4) allows irregular rockhead geometries to be mapped in detail and thus reduces the need for test drilling with its associated high costs. Figure 5.24 shows a typical profile across fluvial

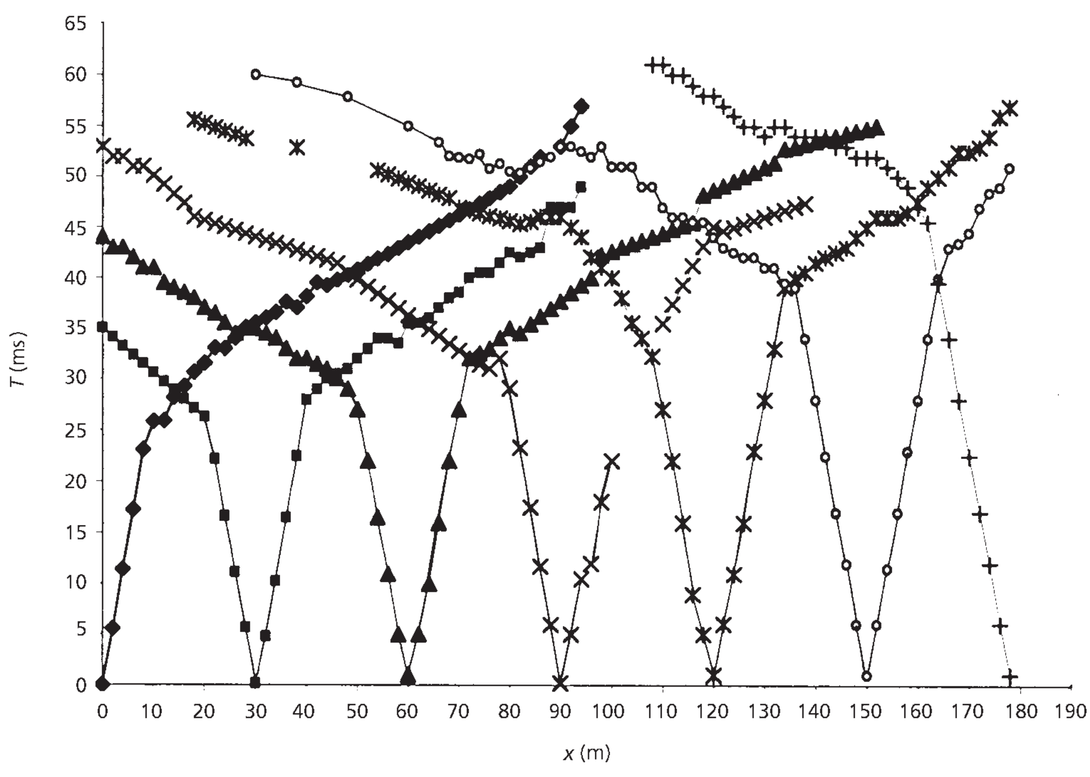

Fig. 5.24 *T–x* graph of a seismic refraction profile recorded over Holocene fluvial sediments overlying Palaeozoic rocks. The geophone separation was 2 m and the shot point separation 30 m. The multiple, overlapping, reversed data allow a continuous plus–minus interpretation of the rockhead interface.

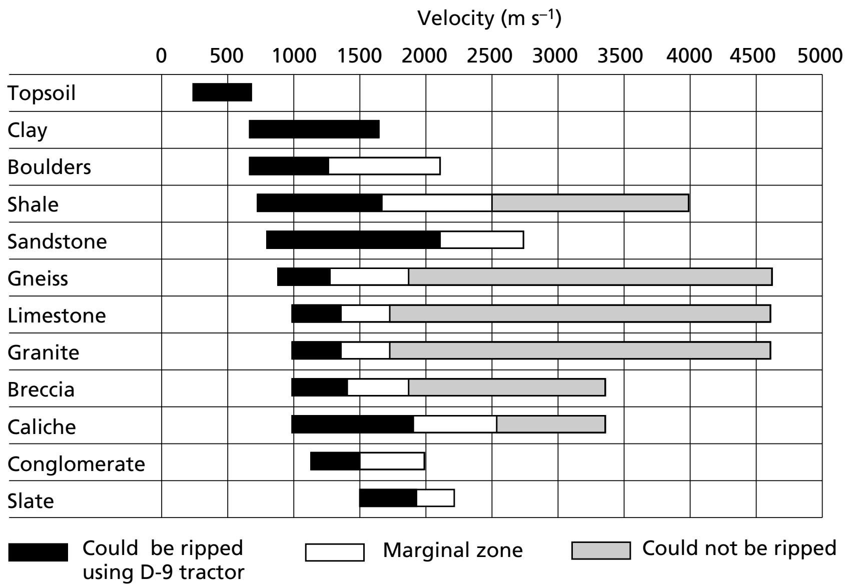

Fig. 5.25 Table showing the variation of rippability with seismic P-wave velocity for a range of lithologies. (After Bell 1993.)

sediments. Here the observation scheme specified a 2 m geophone spacing, and a 30 m shot spacing. The data were recorded with a 48-channel seismograph, with shot points re-fired as the 48 geophones were moved down the profile. The source was a sledgehammer.

The P-wave seismic velocity is related to the elastic constants and the density of the material. It is possible to derive an empirical relationship between the seismic velocity and the 'hardness' of the rock. In engineering usage, an important parameter of rock lithology is its resistance to excavation. If the rock can be removed by mechanical excavation it is termed 'rippable', rather than requiring fracturing by explosives. Empirical tables have been derived relating the 'rippability' of rock units by particular earthmoving equipment to the P-wave seismic velocity. Figure 5.25 shows a typical example of such a table. The range of velocities considered as rippable varies for different lithologies based on empirical averages of such relevant factors as their typical degree of cementation and frequency of jointing. Simple reversed P-wave refraction surveys are sufficient to provide critical information to construction and quarrying operations.

For surveys of near-surface geology, the data collection and interpretation must be efficient and rapid, to make the survey cost-effective against the alternative of direct excavation. The interpretation of seismic refraction profile data is most conveniently carried out using commercial software packages on personal computers. A wide range of good software is available for the plotting, automatic event picking and interpretation of such data. In some situations the option of excavation instead of geophysical survey is very undesirable. Seismic surveys may be used to define the extent and depth of unrecorded landfill sites, or structures on 'brown-field' redevelopments. Commonly seismic and resistivity surveys may be used together to attempt to 'characterize' the nature of the landfill materials. There is an increasing demand for this sort of investigation in many parts of the world.

5.11.2 Hydrological surveys

The large difference in velocity between dry and wet sediments renders the water table a very effective refractor. Hence, refraction surveys find wide application in exploration programmes for underground water supplies in sedimentary sequences, often employed in conjunction with electrical resistivity methods (see Chapter 8). There can, however, be an ambiguity in interpretation of P-wave refraction data since a layer at depth with a velocity in excess of 1500 m s^{-1} could be either the water table, or a layer of more consolidated rock. Recording both P- and S-wave data overcomes this problem, since the water table will affect the P-wave velocity, but not that of the S-waves (Fig. 5.26).

5.11.3 Crustal seismology

The refraction method produces generalized models of subsurface structure with good velocity information,

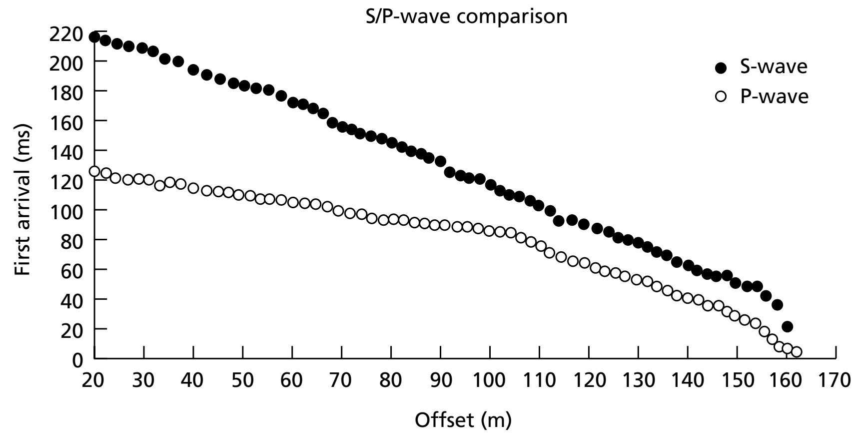

Fig. 5.26 *T–x* graph of a seismic refraction profile with a water-table refractor. The rock unit is the Sherwood Sandstone, having P-wave velocities of 800 and 2000 m s^{-1} for unsaturated and saturated rock respectively (lower line). The equivalent S-wave plot (upper line) shows no effect at the water-table interface.

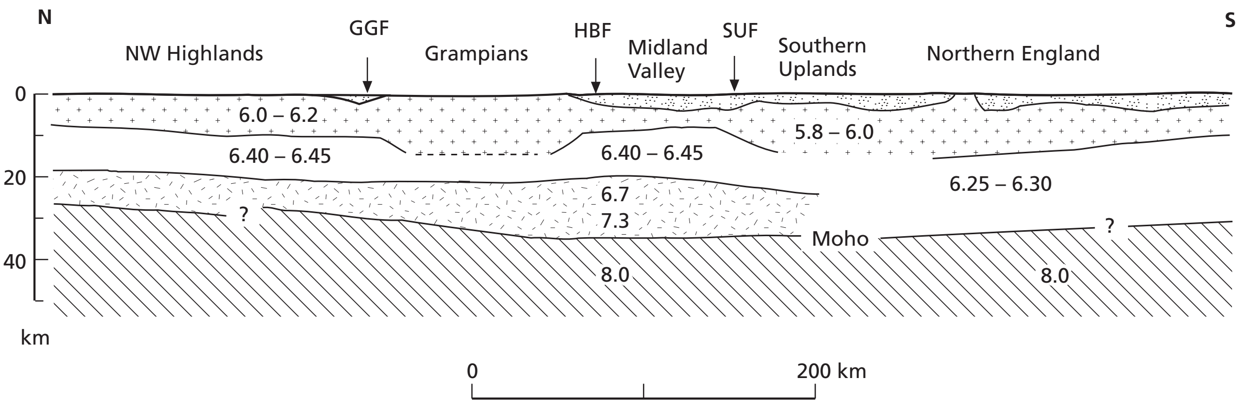

Fig. 5.27 Crustal cross-section across northern Britain based on interpretation of a large-scale seismic refraction experiment. Numbers refer to velocities in km s^{-1}. (After Bamford *et al.* 1978.) Contrast the distance scale with Figs 5.24 and 5.26.

but it is unable to provide the amount of structural detail or the direct imaging of specific structures that are the hallmark of reflection seismology. The occasional need for better velocity information than can be derived from velocity analysis of reflection data alone (see Chapter 4), together with the relative ease of refraction surveying offshore, gives the refraction method an important subsidiary role to reflection surveying in the exploration for hydrocarbons in some offshore areas.

Refraction and wide-angle surveys have been used extensively for regional investigation of the internal constitution and thickness of the Earth's crust. The information derived from such studies is complementary to the direct seismic imaging of crustal structure derived from large-scale reflection surveys of the type discussed in Section 4.16. Interpretation of large-scale refraction and wide-angle surveys is normally carried out by forward modelling of the travel times and amplitudes of recorded refracted and/or reflected phases using ray-tracing techniques.

Large-scale surveys, using explosives as seismic sources, have been carried out to study crustal structure in most continental areas. An example is the LISPB experiment which was carried out in Britain in 1974 and produced the crustal section for northern Britain reproduced in Fig. 5.27.

Such experiments show that the continental crust is typically 30–40 km thick and that it is often internally layered. It is characterized by major regional variations in thickness and constitution which are often directly related to changes of surface geology. Thus, different orogenic provinces are often characterized by quite different crustal sections. Upper crustal velocities are usually in the range 5.8–6.3 km s^{-1} which, by analogy with velocity measurements of rock samples in the laboratory (see Section 3.4), may be interpreted as representing mainly

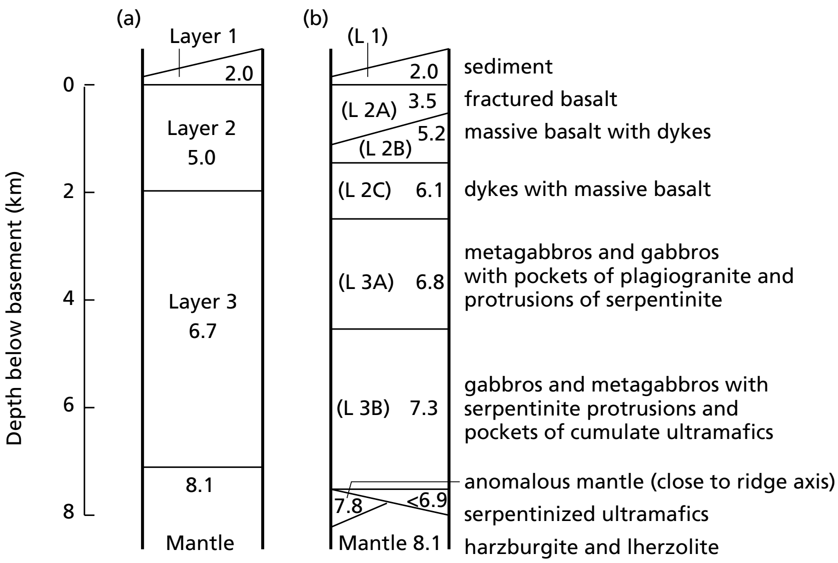

Fig. 5.28 Velocity (km s^{-1}) structure of typical oceanic lithosphere in terms of layered structures proposed in 1965 (a) and 1978 (b), and its geological interpretation. (From Kearey & Vine 1990.)

granitic or granodioritic material. Lower crustal velocities are normally in the range 6.5–7.0 km s^{-1} and may represent any of a variety of igneous and metamorphic rock types, including gabbro, gabbroic anorthosite and basic granulite. The latter rock type is regarded as the most probable major constituent of the lower crust on the basis of experimental studies of seismic velocities (Christensen & Fountain 1975).

5.11.4 Two-ship seismic surveying: combined refraction and reflection surveying

Marine surveys, usually single-ship experiments, have shown the ocean basins to have a crust only 6–8 km thick, composed of three main layers with differing seismic velocities. This thickness and layering is maintained over vast areas beneath all the major oceans. The results of deep-sea drilling, together with the recognition of ophiolite complexes exposed on land as analogues of oceanic lithosphere, have enabled the nature of the individual seismic layers to be identified (Fig. 5.28).

Specialized methods of marine surveying involving the use of two survey vessels and multichannel recording include *expanding spread profiles* and *constant offset profiles* (Stoffa & Buhl 1979). These methods have been developed for the detailed study of the deep structure of the crust and upper mantle under continental margins and oceanic areas.

Expanding spread profiling (ESP) is designed to obtain detailed information relating to a localized region of the crust. The shot-firing vessel and recording vessel travel outwards at the same speed from a central position, obtaining reflected and refracted arrivals from subsurface interfaces out to large offsets. Thus, in addition to near-normal incidence reflections such as would be recorded in a conventional common mid-point (CMP) reflection survey, wide-angle reflections and refracted arrivals are also recorded from the same section of crust. The combined reflection/refraction data allow derivation of a highly-detailed velocity–depth structure for the localized region.

Expanding spread profiles have also been carried out on land to investigate the crustal structure of continental areas (see e.g. Wright *et al.* 1990).

In constant offset profiling (COP), the shot-firing and recording vessels travel along a profile line at a fixed, wide separation. Thus, wide-angle reflections and refractions are continuously recorded along the line. This survey technique facilitates the mapping of lateral changes in crustal structure over wide areas and allows continuous mapping of the types of refracting interface that do not give rise to good near-normal incidence reflections and which therefore cannot be mapped adequately using conventional reflection profiling. Such interfaces include zones of steep velocity gradient, in contrast to the first-order velocity discontinuities that constitute the best reflectors.

Problems

1. A single-ended refraction profile designed to determine the depth to an underlying horizontal refractor reveals a top layer velocity of 3.0 km s^{-1} and a refractor velocity of 5.0 km s^{-1}. The crossover distance is found to be 500 m. What is the refractor depth?

2. What is the delay time for head wave arrivals from layer 3 in the following case?

Layer	Depth (m)	Vel. (km s^{-1})
1	100	1.5
2	50	2.5
3	–	4.0

3. In order that both the horizontal-layer models given below should produce the same time–distance curves for head wave arrivals, what must be the thickness of the middle layer in Model 2?

	Vel. (km s^{-1})	Depth (km)
Model 1		
Layer 1	3.0	1.0
Layer 2	5.0	–
Model 2		
Layer 1	3.0	0.5
Layer 2	1.5	?
Layer 3	5.0	–

4. A single-ended refraction survey (Section 5.3) established to locate an underlying planar dipping refractor yields a top layer velocity of 2.2 km s^{-1} and a downdip apparent refractor velocity of 4.0 km s^{-1}. When the shot point and geophones are moved forward by 150 m, in the direction of refractor dip, head wave arrival times to any offset distance are increased by 5 ms. Calculate the dip and true velocity of the refractor. If the intercept time of the refracted ray travel-time curve at the original shot point is 20 ms, what is the vertical depth to the refractor at that location?

5. A split-spread refraction profile (Section 5.3) with a central shot point is established to locate an underlying planar dipping refractor. The resultant time–distance curves yield a top layer velocity of 2.0 km s^{-1} and updip and downdip apparent velocities of 4.5 km s^{-1} and 3.5 km s^{-1}, respectively. The common intercept time is 85 ms. Calculate the true velocity and dip of the refractor and its vertical depth beneath the shot point.

6. The following dataset was obtained from a reversed seismic refraction line 275 m long. The survey was carried out in a level area of alluvial cover to determine depths to the underlying bedrock surface.

Offset (m)	Travel time (ms)
Forward direction:	
12.5	6.0
25	12.5
37.5	19.0
50	25.0
75	37.0
100	42.5
125	48.5
150	53.0
175	57.0
200	61.5
225	66.0
250	71.0
275	76.5
Reverse direction:	
12.5	6.0
25	12.5
37.5	17.0
50	19.5
75	25.0
100	30.5
125	37.5
150	45.5
175	52.0
200	59.0
225	65.5
250	71.0
275	76.5

Carry out a plus–minus interpretation of the data and comment briefly on the resultant bedrock profile.

7. What subsurface structure is responsible for the travel-time curves shown in Fig. 5.29?

Continued

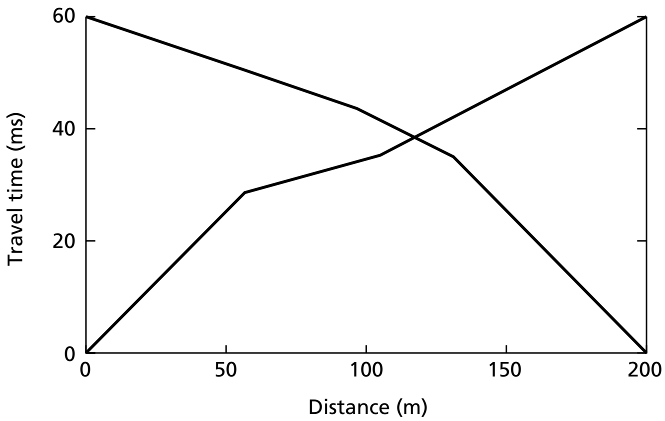

Fig. 5.29 Time–distance curves obtained in the forward and reverse directions along a refraction profile across an unknown subsurface structure.

Further reading

Cardarelli, E. & de Nardis, R. (2001) Seismic refraction, isotropic and anisotropic seismic tomography on an ancient monument (Antonino and Faustina temple AD141). *Geophysical Prospecting*, **49**, 228–41.

Cerveny, V. & Ravindra, R. (1971) *Theory of Seismic Head Waves*. University of Toronto Press.

Dobrin, M.B. & Savit, C.H. (1988) *Introduction to Geophysical Prospecting* (4th edn). McGraw-Hill, New York.

Giese, P., Prodehl, C. & Stein, A. (eds) (1976) *Explosion Seismology in Central Europe*. Springer-verlag, Berlin.

Ivansson, S. (1986) Seismic borehole tomography—theory and computational methods: *Proc. IEEE*, **74**, 328–38.

Palmer, D. (1980) *The Generalised Reciprocal Method of Seismic Refraction Interpretation*. Society of Exploration Geophysicists, Tulsa.

Palmer, D. (1986) *Handbook of Geophysical Exploration: Section 1, Seismic Exploration. Vol. 13: Refraction Seismics*. Enpro Science Publications, Amsterdam.

Sjagren, B. (1984) *Shallow Refraction Seismics*. Chapman & Hall, London.

Stoffa, P.L. & Buhl, P. (1979) Two-ship multichannel seismic experiments for deep crustal studies: expanded spread and constant offset profiles. *J. Geophys. Res.*, **84**, 7645–60.

Willmore, P.L. & Bancroft, A.M. (1960) The time-term approach to refraction seismology. *Geophys. J. R. Astr. Soc.*, **3**, 419–32.